

NJC

Accepted Manuscript



This is an *Accepted Manuscript*, which has been through the Royal Society of Chemistry peer review process and has been accepted for publication.

Accepted Manuscripts are published online shortly after acceptance, before technical editing, formatting and proof reading. Using this free service, authors can make their results available to the community, in citable form, before we publish the edited article. We will replace this *Accepted Manuscript* with the edited and formatted *Advance Article* as soon as it is available.

You can find more information about *Accepted Manuscripts* in the [Information for Authors](#).

Please note that technical editing may introduce minor changes to the text and/or graphics, which may alter content. The journal's standard [Terms & Conditions](#) and the [Ethical guidelines](#) still apply. In no event shall the Royal Society of Chemistry be held responsible for any errors or omissions in this *Accepted Manuscript* or any consequences arising from the use of any information it contains.

A highly selective SBA-15 supported fluorescence “turn-on” sensor for fluoride anion

Richard Appiah-Ntiamoah, Wook-Jin Chung, Hern Kim*

Department of Energy Science and Technology, Energy and Environment Fusion Technology Center,

Myongji University, Yongin, Gyeonggi-do 449-728, Republic of Korea

*Corresponding author: hernkim@mju.ac.kr, Tel: +82 31 330 6688; fax: +82 31 336 6336.

Abstract

In an effort to improve the performance of organic-based F^- receptors, organo-silica receptors are being developed to take advantage of the large surface area that mesoporous silica offers. In this work, we investigated the possibility of using a simple “piece-wise” assembly method to immobilize silyl-ether protected fluorescein isothiocyanate (FITC) molecules (receptor **1**) on the surface of 3-aminopropyltrimethoxysilane (APTES) and 3-[2-(2-aminoethylamino)ethylamino] propyltrimethoxysilan (APAEATMS) modified SBA-15 to form sensors **ASBA** and **TSBA** respectively. We showed that, aqueous solutions of **TSBA** (or **ASBA**) produces distinct changes in absorption and emission spectra upon F^- addition due the F^- directed cleavage of Si-O bonds on receptor **1**. **TSBA** (or **ASBA**) remained stable under prolonged exposure to UV light (losing ~0.12% of its fluorescence intensity), and was highly selective towards F^- over other common anions (Cl^- , Br^- , I^- , HPO_4^{2-} , ACO^- , and NO_3^-). Furthermore, the sensitivity of this type of sensor architecture followed a dependence on the kind of amino-silane compound used, which opens up the possibility of synthesizing sensors with tailored detection limits. The detection limit of **TSBA** and **ASBA** was 0.02 μM and 0.5 μM respectively.

Keywords: Fluorescence; Fluoride; SBA-15; Sensor; Amino-silane

1. Introduction

In recent years, the number and sophistication of non-natural (abiotic) species capable of detecting anions in solution have increased enormously due to fundamental role anions play in a wide range of chemical and biological processes.¹⁻⁵ Among these anions, fluoride, having the smallest ionic radius, highest charge density, and a hard Lewis basic nature, has arisen as an attractive target for sensor designs owing to its association with a diverse array of biological, medical, and technological processes.⁶

Fluoride is used in industrial applications and transformations, especially in steel making and aluminium refining, and it is a well established reagent in organic synthesis.⁷ Novel applications of fluoride have been discovered in the fields of ion batteries,⁸ for enhancing the photocurrent in supramolecular solar cells^{8b} and in ⁹F-PET imaging.^{8c,d}; in the future, it might have a role in the construction of superconducting^{8e} and hydrogen storage materials.^{8f}

Furthermore, it is known that fluoride plays a role in dental health¹⁰ and has potential use for the treatment of osteoporosis.^{11,12} In Anglo-Saxon countries such as U.S.A., U.K., and Australia, water fluoridation, i.e., the addition of fluoride into public water supplies, has been a well established practice since 1945.¹³ However, disagreements on fluoride's allegedly benign health effect on humans, nowadays elicited by mounting evidence of, in fact, its severe toxicity makes it a controversial species.

Through advancement in health sciences, it is now known that fluoride is easily absorbed by the body but excreted slowly. As a result, overexposure to it can lead to acute gastric and kidney problems.¹⁴ Over the years, high concentration of the fluoride anion in the environment and in drinking water has been related to the occurrence of several types of pathologies in humans; such as, osteoporosis, neurological and metabolic dysfunctions, and more recently cancer.¹⁵ As a response to such observations, de-fluoridation treatments and

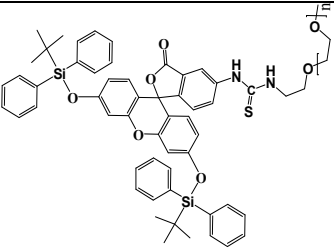
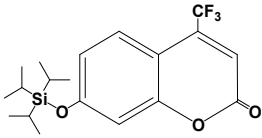
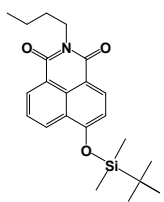
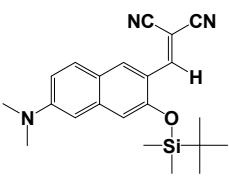
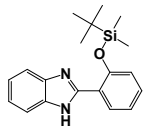
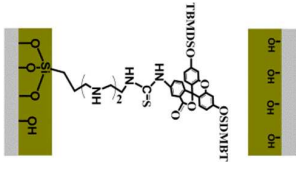
technologies are being developed, among which absorption based processes are the most explored and becoming of wide interest.^{16,17} More generally, there is a growing need for systems capable of recognition, binding and/or sensing of fluoride in a competitive and aqueous environment.

Among several widely used fluoride-detecting and -sensing techniques, including the electrode method,^{18,19} FNMR analysis,²⁰ and colorimetric (UV) and fluorescence sensing, electrochemical systems have become the most well-established. However, this approach has major disadvantages associated with the need for fragile instrumentation and time-consuming manipulations.²¹ In addition; ¹⁹F NMR spectroscopy can be used reliably to detect only micromolar levels of fluoride. Moreover, neither the electrochemical nor the NMR approach can be miniaturized for use in studying biological processes *in vivo*. As a result of these deficiencies, colorimetric and fluorescence sensor systems have attracted the greatest attention because they have been shown to have high sensitivities, with detection limits as low as sub-parts-per-million and the capability of being employed for intracellular fluoride monitoring.⁶

In recent years, several strategies have been developed to design optical sensors for fluoride anions, some including reaction-based chemosensors that utilize F⁻-promoted cleavage reactions; boron-fluoride interaction-based chemosensors; hydrogen-bond and π - π interaction-based chemosensors containing thiourea/urea, amide/sulfonamide, imidazoline/imidazole, indole, pyrrole, Schiff base, and other groups as binding units;⁶ chemosensors bearing metal ion binding sites; and finally chemosensors based on polymers, quantum dots, gold nanoparticles, mesoporous silica, silica particles, and other types of materials.⁶ Amongst all of them, the sensing mode based on a selective F⁻-promoted cleavage reaction exhibits minimum interference from other anions in both aqueous and organic solutions; hence, this

method demonstrates high selectivity and sensitivity for F⁻.

Table 1A comparison of detection limit and response time of **TSBA** with reported probes.

Materials	Detection limit	Detection time	Solv.	Ref.
	0.45 μM	10 min	H ₂ O	39
	50 nM	< 10 sec	AcN	40
	0.59 μM	3 min	AcN	41
	1.43 μM	25 min	DMSO	43
	0.19 μM	40 min	DMF-H ₂ O	44
	0.02 μM	10 min	H ₂ O	Present work

Based on the aforementioned mechanism, a series of receptors have been reported (Table 1) which exhibit impressive detection limits. Because a novel structural or binding motif and

an increased selectivity and/or affinity towards a specific anionic species are some of the features which nowadays make a receptor worthy of the attention of the scientific community, scientist have tried to combine organic-based receptors with inorganic supports in a bit to enhance the performance of such sensor.

Receptors immobilized on inorganic materials such as SiO_2 , Al_2O_3 and TiO_2 have important advantages as solid chemosensors in the heterogeneous solid–liquid phase.^{22,23–30} The immobilized receptors on an inorganic support can liberate the organic guest molecules (metal ions or anions) from the pollutant solution;³¹ the organic–inorganic hybrid nanomaterials can be recycled by suitable chemical treatment;³¹ and lastly, functionalized nanomaterials combined with fluorophores or chromophores display highly selective, sensitive fluorescence or absorption changes compared with spherical structures because of their larger surface areas and well-defined pores.³¹ In this regard, the homogeneous porosity and large surface area of mesoporous silica make it a promising inorganic support.^{29,32} However, only limited examples of such heterogeneous sensors have been reported,^{22,27–30} despite the fact that they take advantage of the independent solubility properties of the receptor in water and organic solvents.

In this article, we investigated the possibility of using a simple assembly method to develop a heterogeneous system for the fluorogenic detection of F^- in total aqueous media. A silyl-ether protected fluorescein isothiocyanate (FITC) molecule (receptor **1**) was assembled in a “piece-wise” manner on the surface of amino-silane modified SBA-15. We show that this sensor architecture is highly photostable and demonstrates beneficial properties, such as: high sensitive and selective towards F^- in total aqueous media: its detection limit values are comparable to purely organic-based sensors reported in literature; simple preparation method; and, an architect which offers the opportunity of using different kinds amino-alkoxysilane

coupling agents to vary its detection limit.

2. Experimental

2.1. Materials

All chemicals and reagents were purchased from Acros and Sigma Aldrich Chemical Co. and were used as received without further purification. The reagents used were as follows: 3-aminopropyltriethoxysilane (APTES, 97.0%), 3-[2-(2-aminoethylamino)ethylamino] propyltrimethoxysilane (APAEATMS, 97.0%), fluorescein 5(6) Isothiocyanate (FITC, $\geq 90.0\%$), anhydrous acetonitrile (99.8%), anhydrous toluene (99.8%), anhydrous DMSO (99.9%), anhydrous DCM (99.8%), absolute ethanol (99.5%), tetrabutylammonium fluoride hydrate (98%), tetrabutylammonium nitrate (97%), tetrabutylammonium iodide (98.0%), tetrabutylammonium chloride hydrate (98.0%), tetrabutylammonium bromide ($\geq 98.0\%$), triethylamine ($\geq 99.0\%$), tetrabutylammonium phosphate monobasic ($\geq 99.0\%$), tetrabutylammonium acetate ($\geq 97.0\%$), trifluoromethanesulfonic acid tert-butyldimethylsilyl ester (TBMD-OTf, 97.0%), 1.0 M HEPES buffer solution in water, and deionized water ($>18.0 \text{ M}\Omega \text{ cm}$), from a Milli-Q system (Millipore, Bedford, M.A, USA). Pure SBA-15 was synthesized according to the method reported in literature.³³

2.2. Characterization

The FT-IR spectra of the organic moieties used and SBA-15 were recorded on a Varian FTS 2000 Fourier Transform Infrared (FT-IR) spectrometer using KBr-pellet method; while, elemental compositional analysis was carried out via Dispersive X-Ray spectrometry (EDX) with a scanning electron electrode at 20 kV. Nitrogen adsorption-desorption isotherms were

conducted at 78 K on a Micromeritics ASAP 2010 analyzer to measure changes in pore diameter, pore volume, and surface area of **SBA-15**, **ASBA**, and **TSBA**. Thermal gravimetric analysis (TGA) was conducted on a Perkin-Elmer TGA-7 instrument to measure the % weight (wt%) loss of each sample at a heating rate of $10\text{ }^{\circ}\text{C min}^{-1}$ using a Pt pan in N_2 flowing at 50.0 ml min^{-1} . Heating temperature was scanned from $30\text{ }^{\circ}\text{C}$ to $900\text{ }^{\circ}\text{C}$. Emission and absorption Spectra change in **ASBA**, and **TSBA** after anion titration was measured on a Hitachi F-4600 fluorescence spectrometer and a Cary 100 UV-Visible spectrophotometer. The same fluorescence spectrometer was used to investigate the stability of the sensors after being exposed to a 30W UV-light for a prolonged period of time. A Viber Lourmat UV lamp (VL-215.BL, 30W, 356 nm) was used to show the color change of the sensor before and after anion titration.

2.3. Synthesis of SBA-15

The method used to synthesize SBA-15 followed that reported in literature.³³ In a typical procedure, 325.0 ml of distilled water was heated and maintained at 40°C , while under constant stirring (800 rpm), before adding 60.0 ml of HCl. 10.0 g of copolymer surfactant P123 and water were then added to the solution and stirred at 800 rpm until a clear solution was obtained. Next up, 20.6 g of TEOS was added to produce a white-homogeneous solution, which was kept at the same temperature and stirring rate for 1~2 h until a precipitation was formed. The suspension was then stirred, at steady-state, for 24 h, which was followed by another round of stirring for 24 h stirring but at 80°C . Hot water (at 40°C) was used to vacuum filter the white precipitate repeatedly. The purified white solid then air dried for 5 days. Finally the dried sample was calcined at $500\text{ }^{\circ}\text{C}$ for 5 h at a heating rate of $2.5\text{ }^{\circ}\text{C min}^{-1}$.

2.4. Synthesis of ASBA and TSBA

2.4.1. Silanization of SBA-15 with amino-functional trimethoxysilanes

The silanization method used was essentially similar to that reported in literature,³⁴ except that, the ratio of SBA-15 to APAEAETMS (or APTES) was changed. Briefly, 2.0 g of SBA-15 was mixed with 2.0 g of APAEAETMS (or APTES) in 50.0 ml dry toluene and agitated under reflux (at 110 °C) for 43 h in N₂ atmosphere. The modified silica nanoparticles were then isolated and purified 6 times with toluene, ethanol, and diethylether by centrifugation/redispersion processes (for 30 min at 16,000 rpm) to remove unreacted and loosely bound APAEAETMS (or APTES). Finally, the purified solid was cured at 80 °C for 6 h in a conventional oven after which it was cooled in a desiccator. **TM** (or **AP**) was used to denote the cured solid.

2.4.2. “Piece-wise” assembly of receptor 1 on **TM** (or **AP**)

2.4.2.1. Immobilization of FITC on **TM** (or **AP**)

0.5 g of **TM** (or **AP**) was dissolved in 30.0 ml of absolute ethanol and stirred for 10.0 min, after which a calculated amount of FITC [1.5 fold excess relative to the amount of grafted APAEAETMS (or APTES)] was added to the suspension. The resulting mixture was stirred for 24 h in the dark at room temperature. The resulting red product was collected and washed copiously (for 1 h at 16,000 rpm, 4 times) with absolute ethanol until the filtrate was clear of color. Finally, the purified solid was oven dried at 80 °C for 1h and was denoted as **TM-FITC** (or **AP-FITC**).

2.4.2.2. Silylation of phenol groups on **TM-FITC** (or **AP-FITC**) with TBMD-OTF

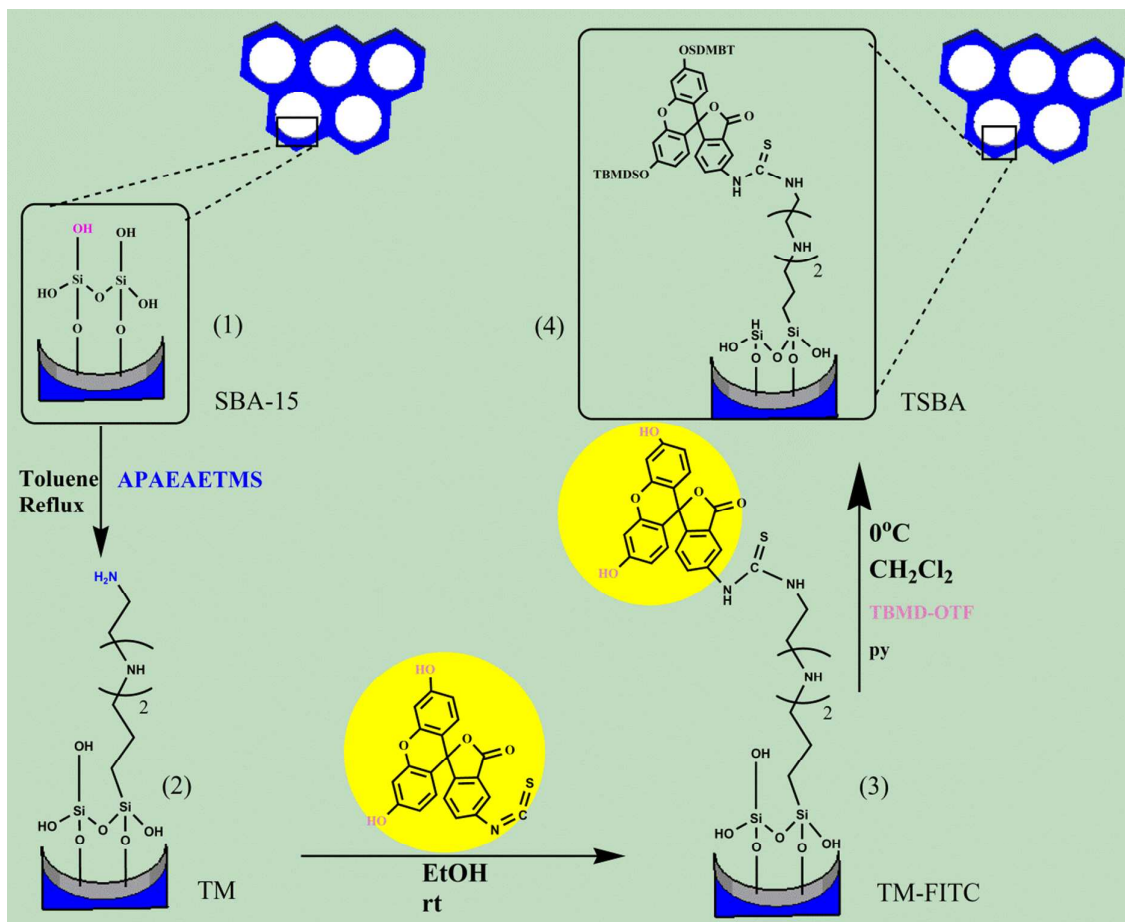
A mixture of **TM-FITC** (or **AP-FITC**) (0.2 g), anhydrous DCM (20.0 ml), and pyridine

(2.0 ml) was stirred under nitrogen atmosphere for 30.0 min, while the beaker was immersed in a mixture of cracked ice and water. A calculated amount of TBMD-OTF [2.5 fold excess relative to the amount of grafted **FITC**] was added to the suspension stirred for an additional 5 h. The light yellow product was then filtered and washed several times with acetonitrile and water. The purified sample was dried under vacuum for 48 h at room temperature. The final product was denoted as **TSBA** (or **ASBA**).

3. Results and discussion

3.1. Characterization of sensor

Receptor **1**, having TBMD-OTF and FITC components as the trigger and fluorescent unit respectively, was synthesized via a 2-step assembly reaction on amino-modified SBA-15 to produce sensors **TSBA** and **ASBA** as shown in Scheme **1**. The structure and functionality of the sensors was confirmed by FT-IR, EDX, thermogravimetry, BET, and BJH analysis. SBA-15 was synthesized according to the procedure described in literature³³ as shown in the experimental section.



Scheme 1 Synthesis route to TSBA.

3.1.1. TG analysis of immobilized organic moiety loading

Data from the TG analysis was used to trace each synthesis steps and also calculate the wt% loss due to receptor **1**. The latter was used to estimate the effect of steric hindrance on the loading density of receptor **1**, and the correlation this might have with the sensing ability of the sensor.

As expected, the thermogram of **TSBA** displayed three distinct weight loss regions

which suggested that the organic moieties had been successfully immobilized (Fig. 1). Like most ⁴³silica supports, **TSBA**'s first weight loss of ~2% from 30-103°C was due to the evaporation of physically trapped water. The second loss of ~5w% (associated with APAEAETMS with a bp of ~118°C) occurred ~105-310°C, while the final weight loss of ~22.69wt% (associated with receptor **1**) occurred ~310-685°C. Losses above 700°C were not considered since this is caused by the degradation of intraglobulated silanol groups.⁴³ The inflection points at which the respective weight losses were calculated are shown in Fig. S3.

A similar result was obtained for **ASBA**, except that its final weight loss of 27.56% was higher than that of **TSBA**, which suggested that the latter has a higher density of receptor **1** on its surface than the former. This makes sense since APAEAETMS is bulkier than APTES. The above calculations were done under the assumption that, no leaching occurred during the heating process.

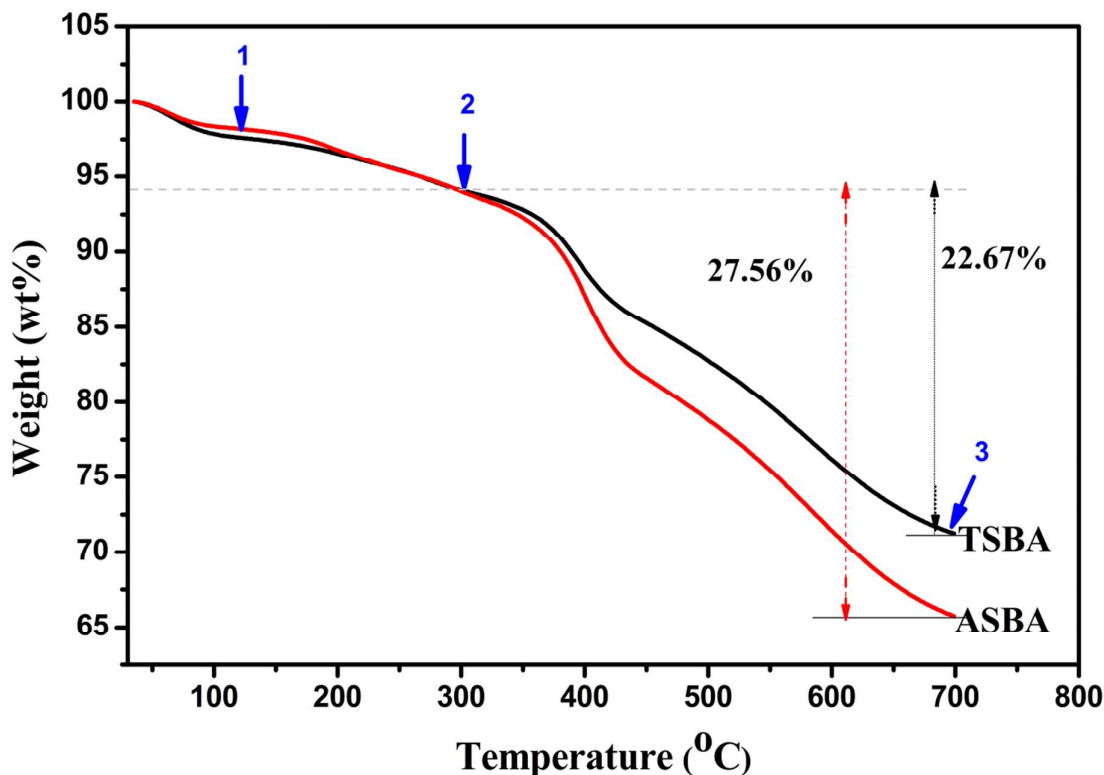


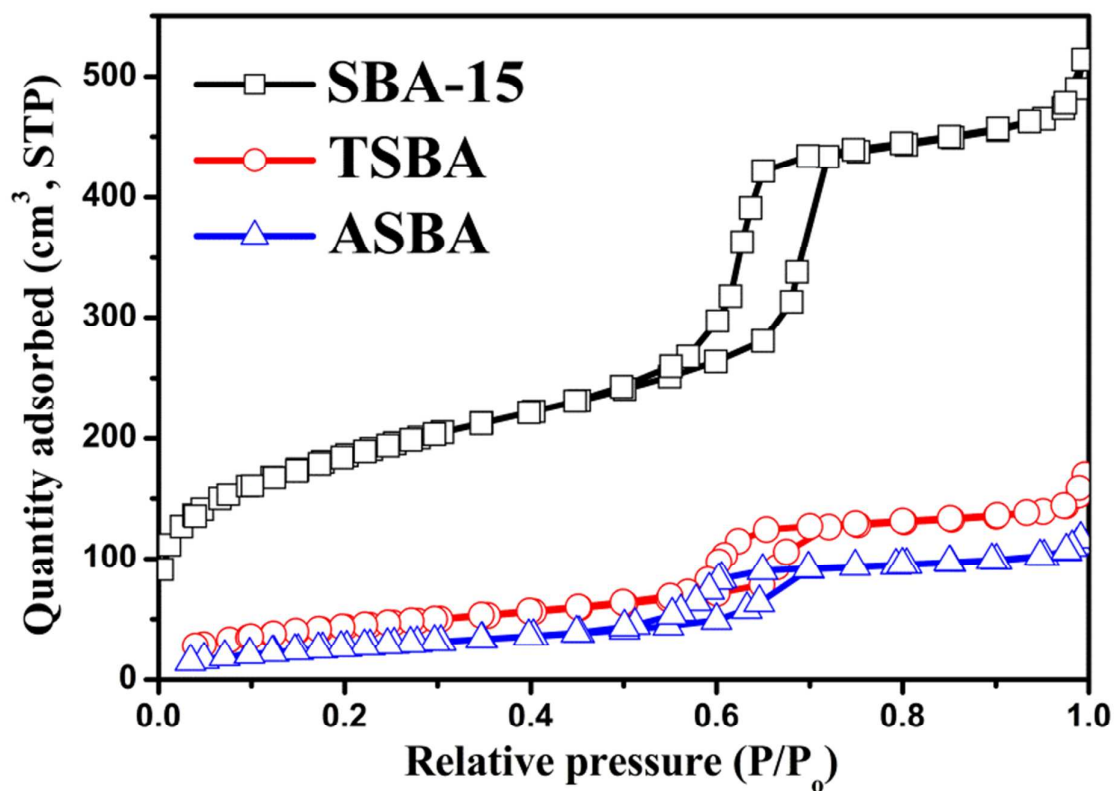
Fig. 1 Thermogravimetric analysis of ASBA and TSBA.

3.1.2. Surface group analysis

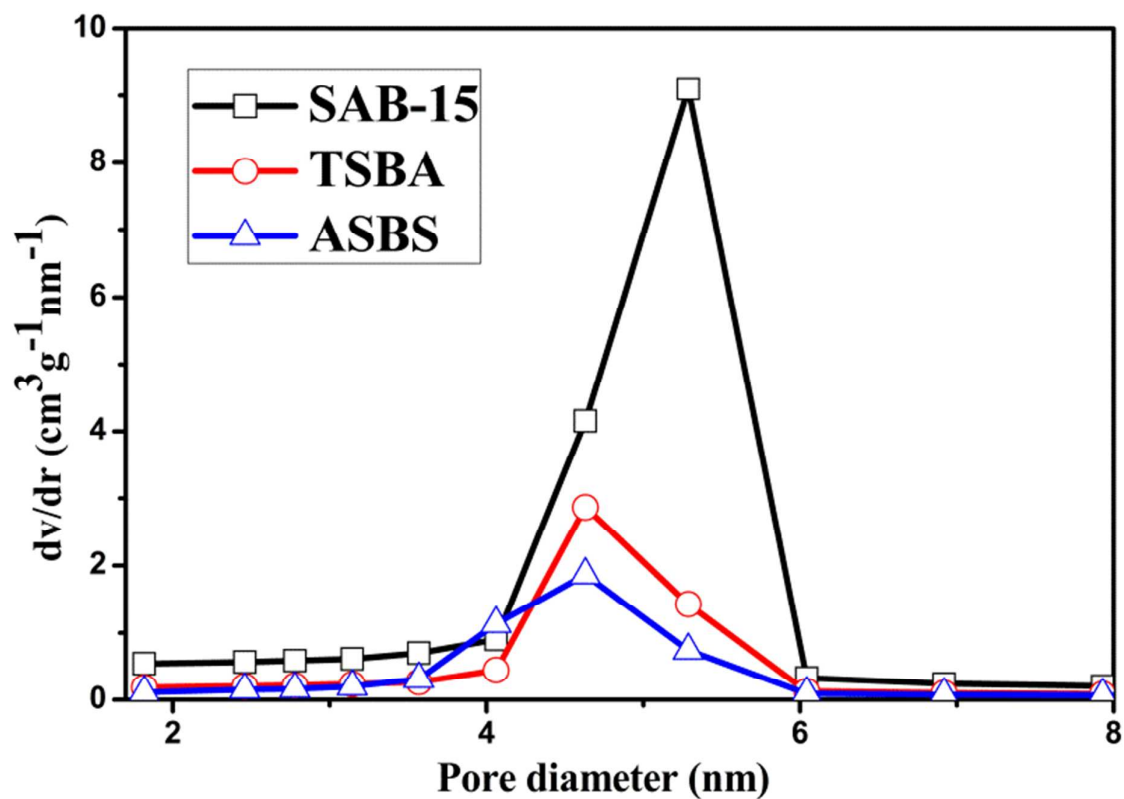
The TGA results were put to the test by analyzing key characteristics of SBA-15, ASBA, and TSBA, namely the BET surface area (S_{BET}), pore diameter (d_{BJH}), and pore volume (V_{p}) as shown in Fig. S1. It is clear that the surface properties of SBA-15 were affected by the immobilization reactions: N_2 adsorption and desorption (Fig. S1(a)) reduced drastically after immobilization with ASBA showing the greatest effect. The S_{BET} of SBA-15 was $700.85 \text{ m}^2 \text{ g}^{-1}$, which is ~ 8 and ~ 7 times that of ASBA and TSBA respectively (Table 2). A similar trend was observed for pore volume (V_{p}): 0.80, 0.20, and $0.12 \text{ cm}^3 \text{ g}^{-1}$ were the respective values.

As expected, the grafting reaction also led to a reduction of the pore diameter, as shown in Fig. S1(b) with ASBA showing the least value. This is typical of porous silica substrates

with high loading.⁴⁴ The above results corroborated that of the TGA analysis and strongly indicated the grafting reaction was successfully done. Elemental analysis was carried out to confirm the aforementioned results, and also calculate the percentage elemental distribution over SBA-15, ASBA, and TSBA.



(a)



(b)

Fig. S1 (a) Nitrogen adsorption–desorption isotherms and (b) Barrett–Joyner–Halenda (BJH) pore diameters of SBA-15, ASBA, and TSBA.

Table 2 Barrett–Joyner–Halenda pore diameter (d_{BJH}), Brunauer–Emmett–Teller surface area (S_{BET}), and pore volume (V_{p}) of SBA-15, TSBA, and ASBA.

Material	d_{BJH} (nm)	S_{BET} ($\text{m}^2 \text{g}^{-1}$)	V_{p} ($\text{cm}^3 \text{g}^{-1}$)
SBA-15	5.30	700.85	0.80
TSBA	4.64	100.81	0.20
ASBA	4.59	89.51	0.12

Table 3 gives a summary of elemental mapping results obtained via energy dispersive X-ray spectroscopy (EDX). Unlike in **ASBA**, and **TSBA**, Carbon (C) and sulfur (s) atoms are clearly absent in pristine SBA-15, which indicated that the grafting reaction was successful. Furthermore, for the same mass of sample analyzed, the amount of sulfur (s), silicon (Si), and oxygen (O) on **ASBA** was greater than that on **TSBA**, which confirms that the former had more **receptor 1** molecules on its surface than the latter.

Table 3

EDX for as-prepared SBA-15, TSBA, and **ASBA**.

Sample	Weight %				Atomic%			
	Carbon	Oxygen	Silicon	Sulfur	Carbon	Oxygen	Silicon	Sulfur
SNP	-	64.06	35.94	-	-	73.58	26.42	-
TSBA	49.50	40.62	8.90	0.98	61.01	34.43	3.96	0.60
ASBA	38.22	46.75	10.1	1.57	53.91	40.22	4.47	1.4

The formation of new bonds on SBA-15 and **TSBA** was also confirmed via the FT-IR spectroscopy (as shown in Fig. 2). The peaks at 3437, 1632, 954 cm^{-1} were due to the stretching (3437 cm^{-1}) and bending (1632 cm^{-1}) vibrations of silanol groups and physically absorbed water.^{33,34} In both samples, the characteristic Si-O-Si peaks at ~1080, 810, and 451 cm^{-1} were present, which confirmed the formation of a condensed silica network.³⁴ Furthermore, the spectra of **TSBA** showed new peaks at ~3000-2800 cm^{-1} which are

characteristic of aliphatic-alkyl-chain C-H vibrations. Also found was N-H bending vibrations around 34680 cm^{-1} and -NH deformation vibrations at around 341530 cm^{-1} . Furthermore, new peaks belonging to the aromatic ring of FITC appeared at around 1620-1303 cm^{-1} . The aromatic C-H stretching vibration appeared at around 194-902 cm^{-1} . Also, the aliphatic CH stretching vibration peak at $\sim 2924\text{ cm}^{-1}$ intensified after the silylation reaction, which signified the presence of C-H groups belonging to TBMD-OTF. However, the lactone and thione (-C=S) peaks were over shadowed by the much dominant FITC and Si-O-Si peaks respectively. The above results confirmed that the receptor **1** was covalently bonded to the surface of TSBA.^{37,38}

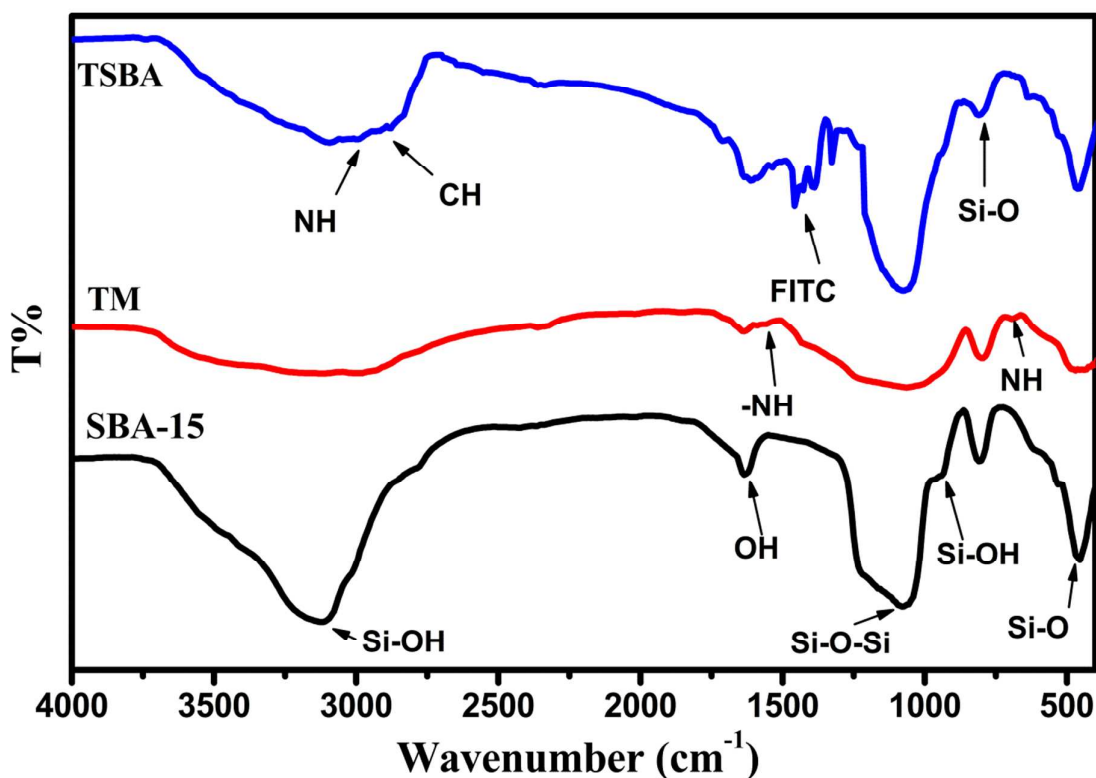
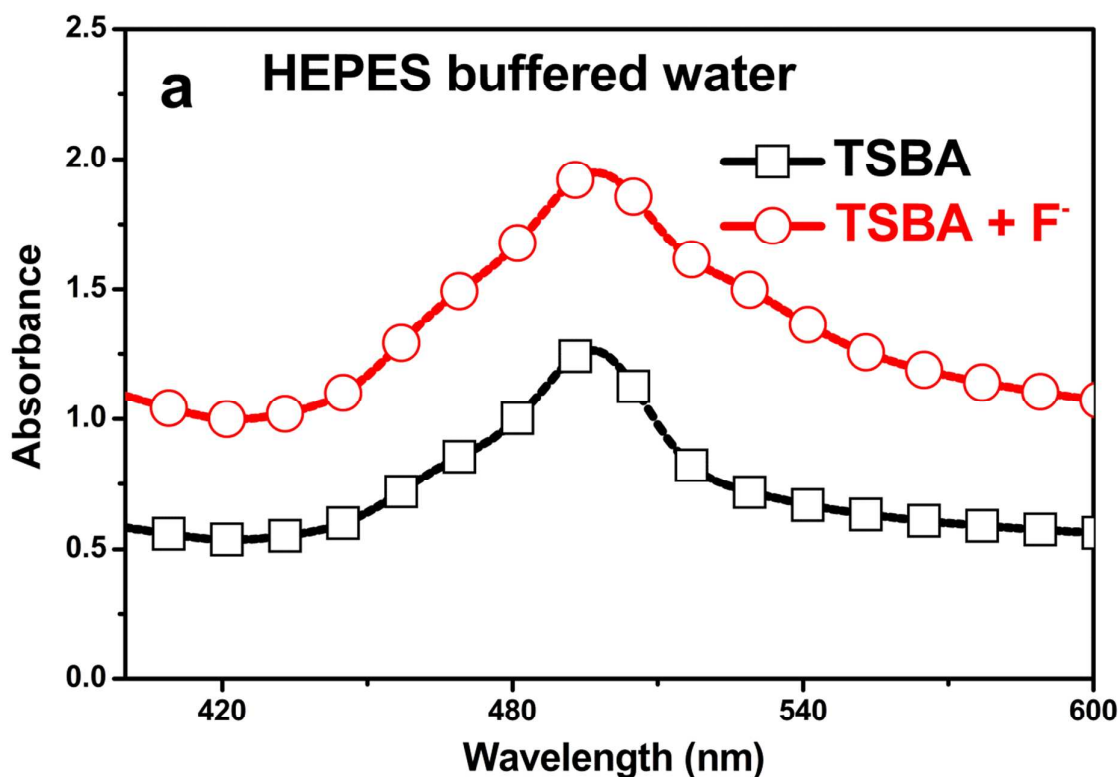


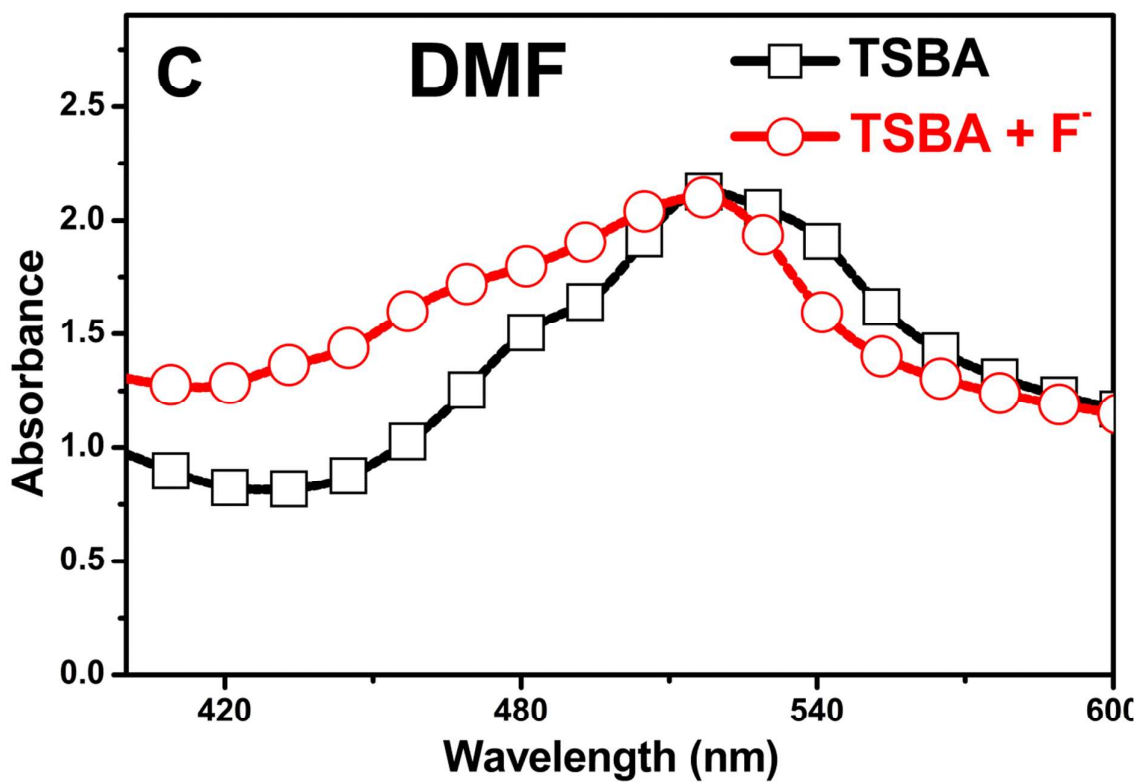
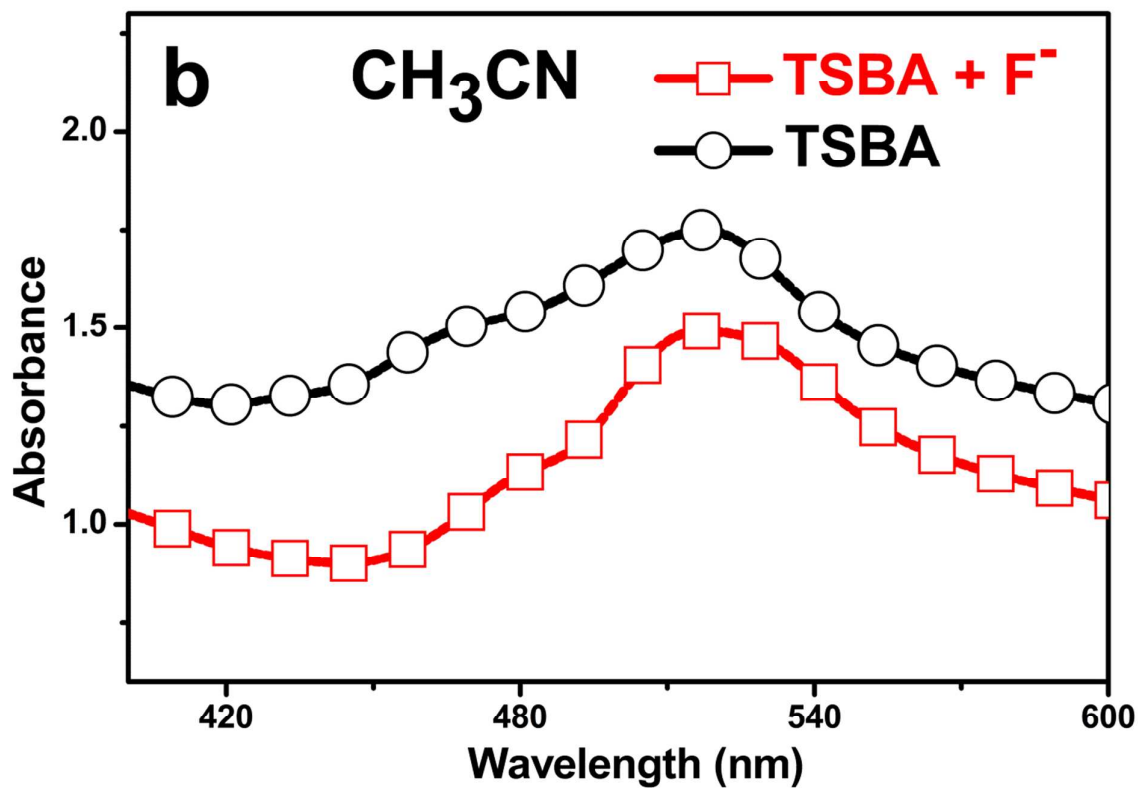
Fig. 2 IR spectra of SBA-15, TM, and TSBA

3.2. Performance of evaluation of sensor

3.2.1. Detection condition and kinetic studies

The detection environment influences the optical response of optical sensors.^{39,40} Thus, the optical response of **TSBA** towards F^- (1.5 equiv.) in different solvents was first studied. As shown in Fig. S2, **TSBA** exhibited a mark increase in absorption in pH 7.4 HEPES buffered water, while the others (CH_3CN , DMF, EtOH, and DMSO) showed either a decrease or unchanged absorbance. This was welcome news as only a few sensors work in total aqueous media (Table 1). The pH 7.4 HEPES buffered water was chosen as the detection medium for further studies.





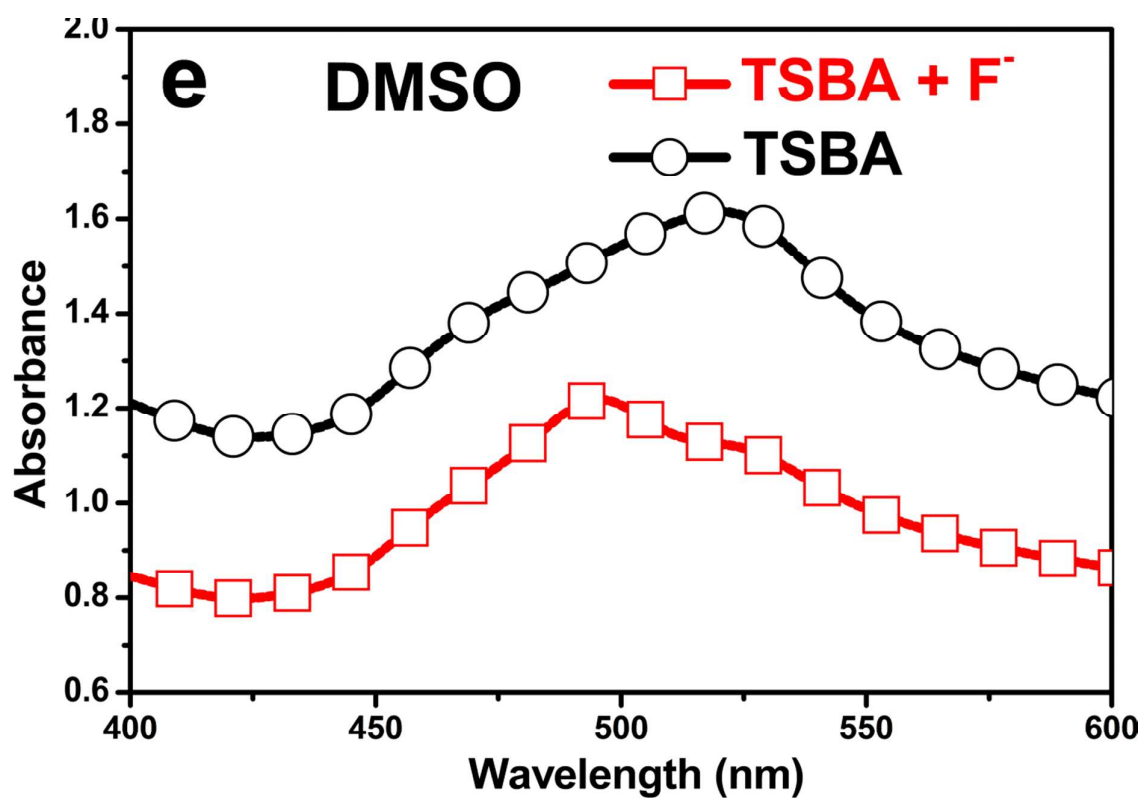
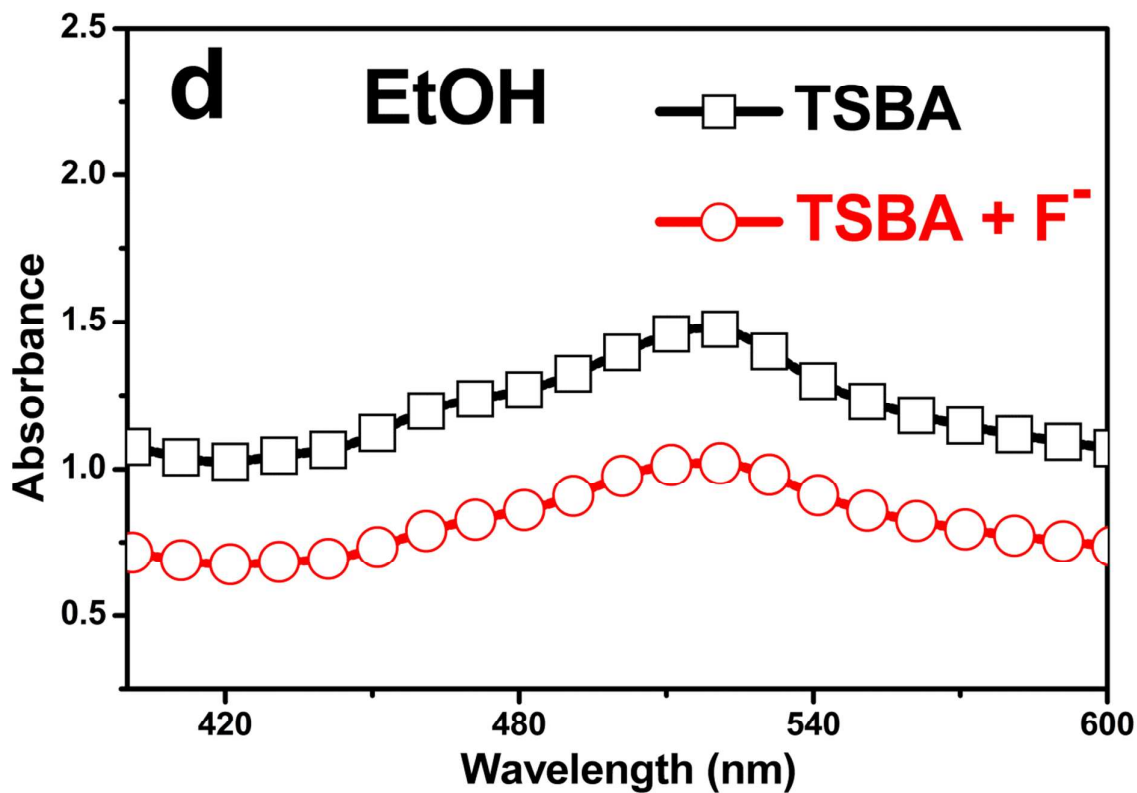


Fig. S2 Absorbance spectra of **TSBA** (88.0 mg mL^{-1}) and **TSBA** + F^- in different solutions of (a) pH 7.4 HEPES buffered water, (b) CH_3CN , (c) DMF, (d) EtOH, and (e) DMSO). ($[\text{F}^-] = 1000 \text{ } \mu\text{M}$)

The properties of optical sensor are evaluated based on their emission and absorption intensity values; thus, it was critical to investigate the equilibrium reaction time (kinetics) between **ASBA** and **TSBA**, and F^- . To do this, the fluorescence intensity variation as a function of time upon addition of fluoride anion was measured as shown in Fig. 3. The fluorescence intensity value was observed to reach a maximum within 7 min, which suggested that both sensors were equally very responsive towards fluoride anion. All subsequent intensity changes were measure after 7 min.

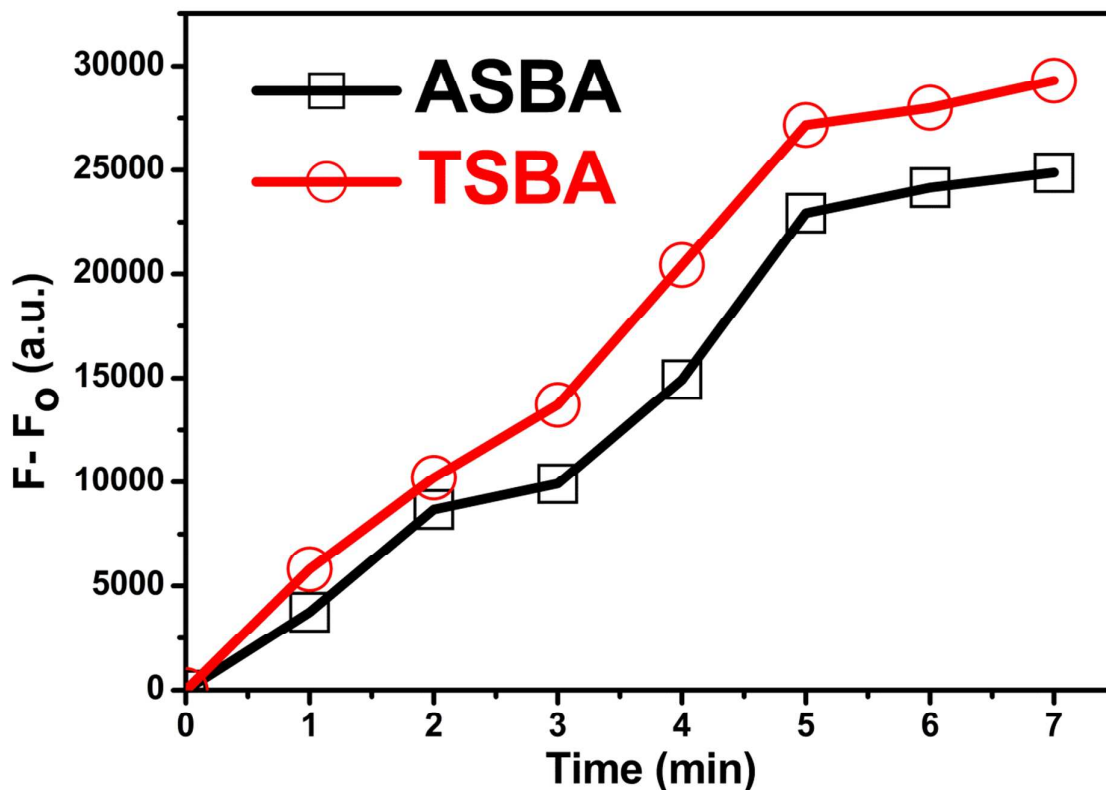
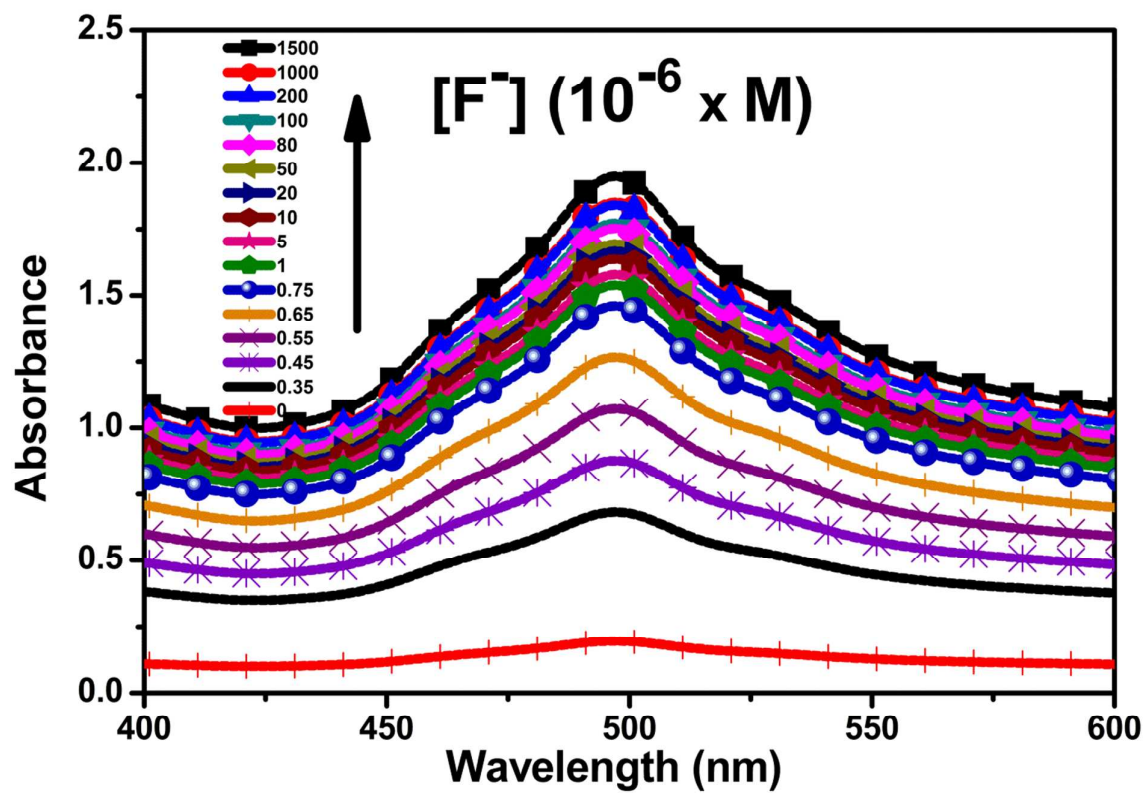


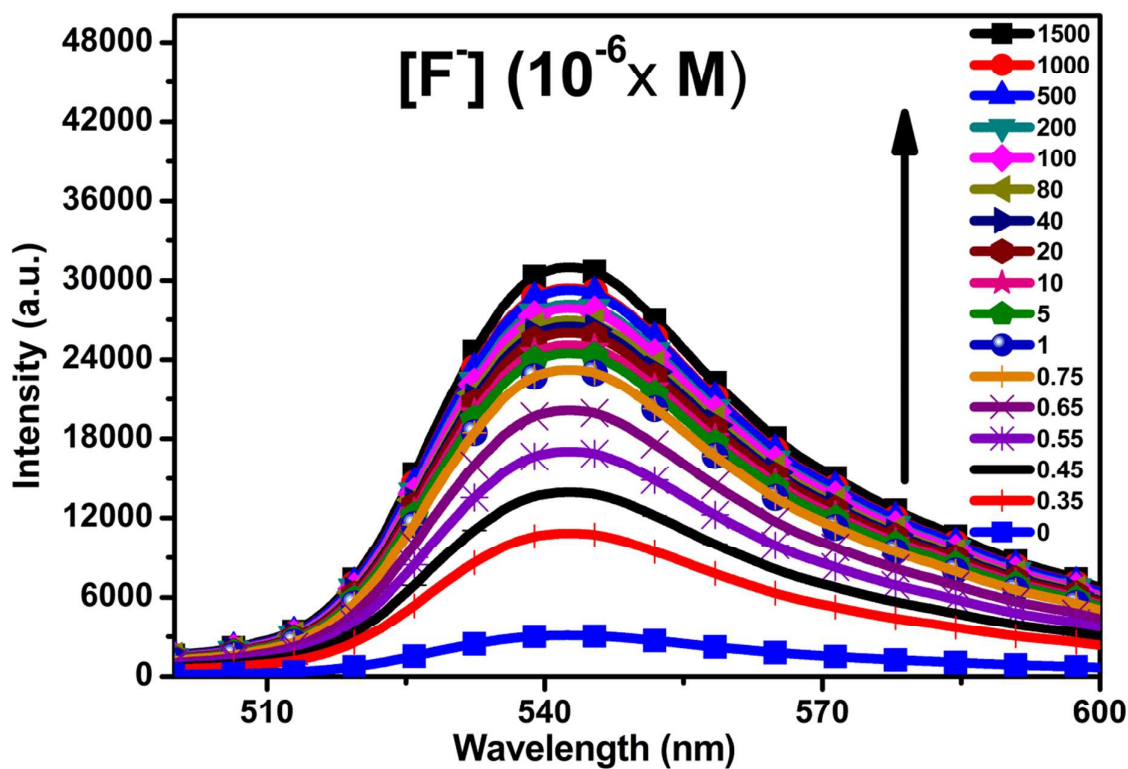
Fig. 3 Fluorescence intensity increment ($F-F_0$) of **ASBA** (88.0 mg mL^{-1}) and **TSBA** (72.0 mg mL^{-1}) recorded at 526 nm at different times upon adding $1.000 \mu\text{M}$ of F^- in pH 7.4 HEPES buffered water ($\lambda_{\text{ex}} = 496 \text{ nm}$).

3.2.1. Anion sensing via fluorescence “turn-on” in total aqueous medium

The emission and absorption spectra of **TSBA** in pH 7.4 HEPES buffered water after the addition of different $[\text{F}^-]$ are displayed in Figs. 4. The intensity values were observed to be very low in the absence of F^- as well as at low $[\text{F}^-]$; however, as the F^- concentration increased, the fluorescence and absorption intensity values increased by 20-fold (at 526 nm) and 30-fold (496 nm) respectively until equilibrium was reached $\sim [\text{F}^-] = 1000 \mu\text{M}$.



(a)



(b)

Fig. 4 (a) Absorption and (b) Fluorescence spectra changes in TSBA (88.0 mg mL^{-1}) upon addition of increasing concentration of F^- (as its TBA salt, 0.0 to 1.5 equiv) in 7.4 pH HEPES buffered water. $\lambda_{\text{ex}} = 496 \text{ nm}$ was used for the fluorescence experiment.

Job's plot was used to investigate the stoichiometric relationship between $[\text{F}^-]$ and receptor **1** at this concentration (Fig. 5). A maximum at 0.5 M fraction of receptor **1** indicated that, the stoichiometric ratio was 1 : 1.

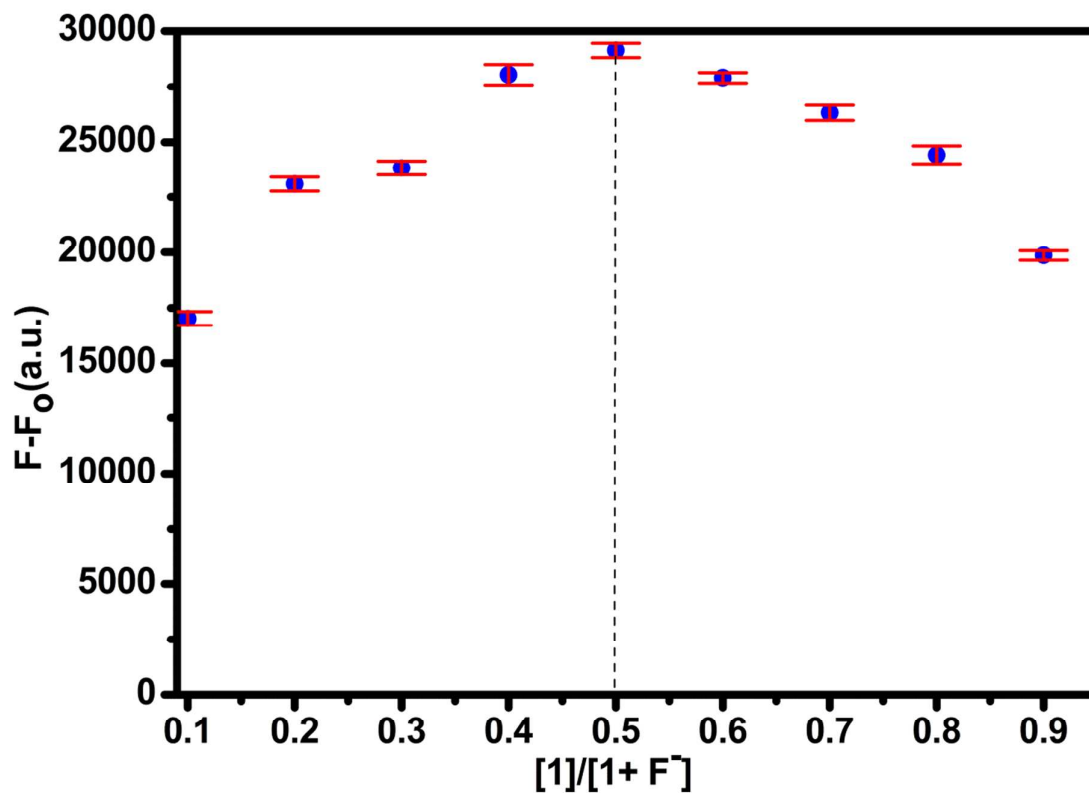
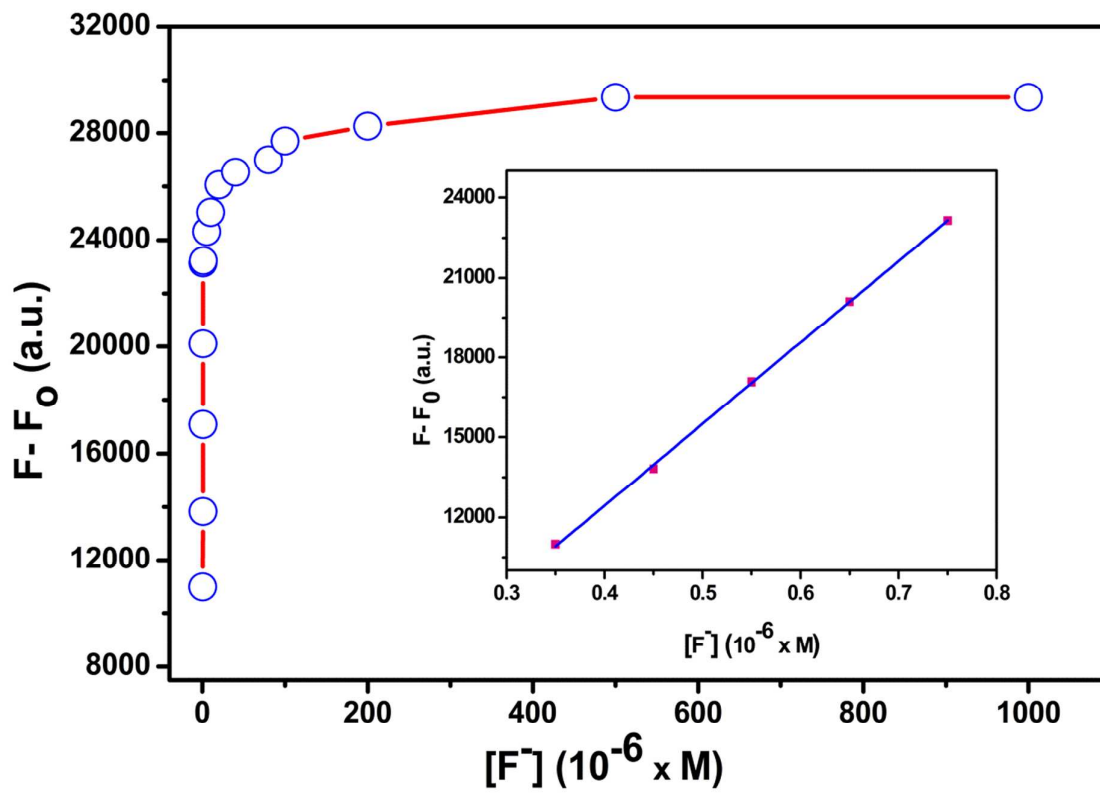
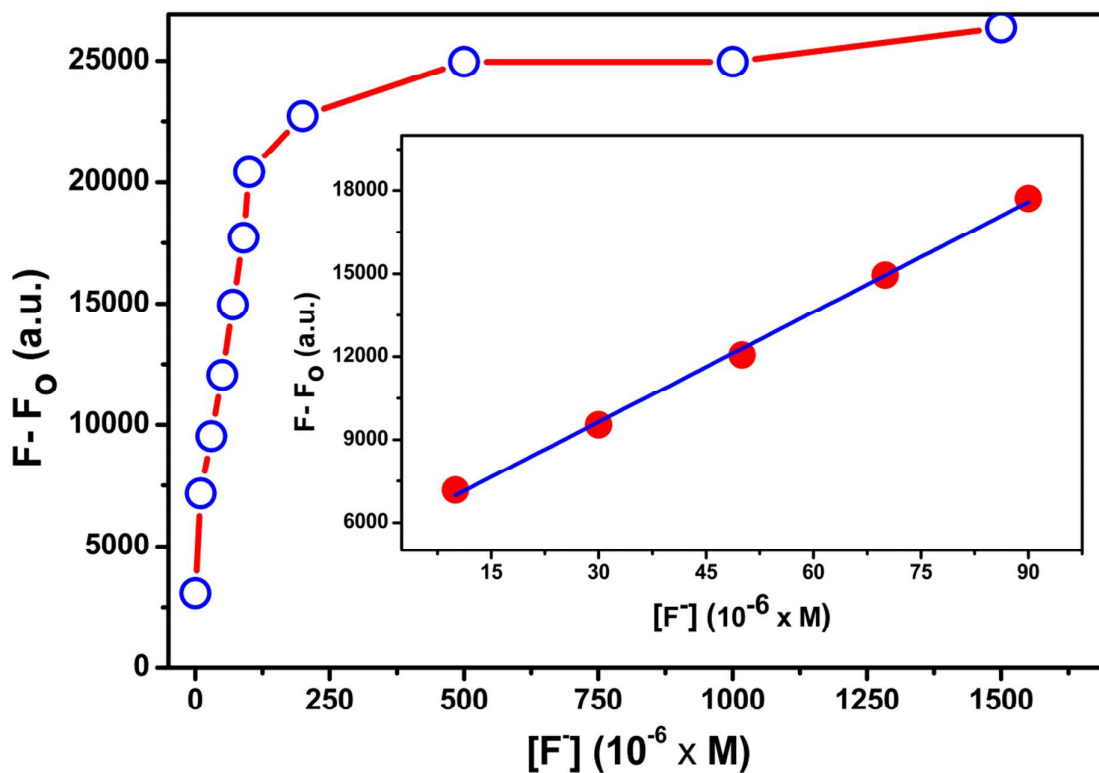


Fig. 5 Job's plot for the reaction between receptor 1 and TBAF in 7.4 pH HEPES buffered water with $[1 + F] = 1000\mu\text{M}$. A maximum value at 0.5 is seen, which is consistent with a 1:1 stoichiometric reaction.

A working curve based on fluorescence intensity increment at 526 nm with increasing F concentrations was established, as shown in Fig. S4. A steep increase in fluorescent intensity was observed in the concentration range of 0-100 μM , and a linear response was observed between 0.2 μM and 0.75 μM (insert of Fig. S4(a)). Based on the linear correlation, the detection limit of **TSBA** was calculated as 0.02 μM using the method described in literature.⁴¹



(a)



(b)

Fig. S3 (a) Fluorescence intensity increment ($F - F_0$) of **TSBA** (88.0 mg mL⁻¹) at 526 nm at different concentrations of F^- (0.0-1500 μM) in pH 7.4 HEPES buffered water (λ_{ex} = 496 nm). Insert: enlarged figure in the concentration range of 0.2-0.75 μM of fluoride anion and (b) Fluorescence intensity increment ($F - F_0$) of **ASBA** (72.0 mg mL⁻¹) at 526 nm at different concentrations of F^- (0.0-1500 μM) in pH 7.4 HEPES buffered water (λ_{ex} = 496 nm). Insert: enlarged Figure in the concentration range of 10.0-90.0 μM of fluoride anion.

Similarly, the detection limit for **ASBA** was calculated as 0.50 μM using data from Fig. 6 and Fig. S4 (b). The **ASBA** solution used to obtain the spectra in Fig. D contained the same moles of receptor **1** as that of the **TSBA** solution used earlier; hence, a similar fluorescence spectrum was expected. However, the maximum fluorescence intensity of **ASBA** was found to be 1.2 times lower than that of **TSBA** (ca. 29344.646 and 24900.5266 respectively). Also, noticeable fluorescence change in **ASBA** begun at $[\text{F}^-] = 10 \mu\text{M}$.

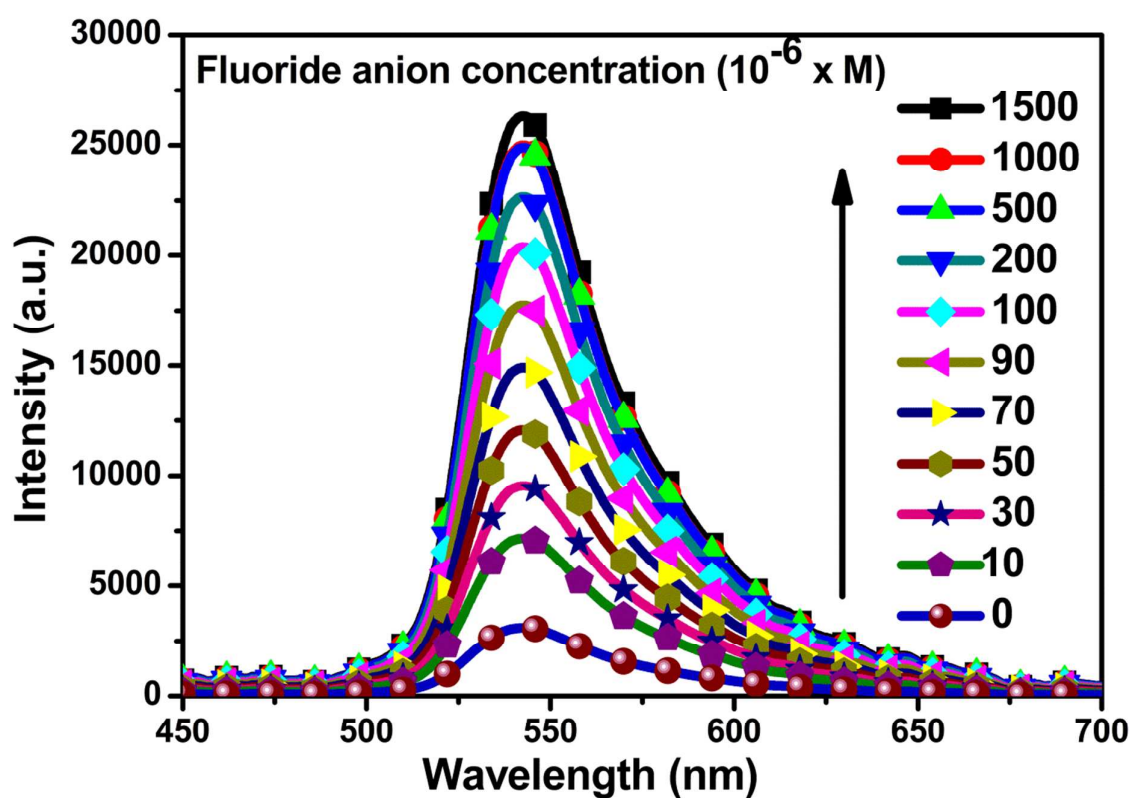


Fig. 6 Fluorescence spectra of **ASBA** (72.0 mg mL^{-1}) in 7.4 pH HEPES buffered water upon addition of different amount of F^- .

That notwithstanding, the detection limit results obtained for **TSBA** and **ASBA** are

amongst the best reported in literature, as shown in table 1. The other remarkable observable feature is the mark difference in detection limit displayed by the two sensors, which differ only by receptor **1** loading densities dictated by amino-silane compounds. The secret to the detection limit difference might lie in the spatial and charge transfer relationship between receptor **1** and F⁻.

We used FT-IR spectroscopy to investigate the reaction between **TSBA** with fluoride ions. A solution of 1500 μM TBAF was titrated against a **TSBA** solution (88.0 mg mL⁻¹ in 7.4 pH HEPES buffered water) added under stirring. After seven minutes, the suspension was centrifuged and the solid residue was dried and directly used FT-IR measurement. The spectrum is shown in Fig. S4. From this figure, it appears the Si-O-Si band at $\sim 1080\text{ cm}^{-1}$ had narrowed, suggesting the loss of Si-O groups belonging to the cleaved TBMD-OTF group. Additionally, the aliphatic C-H vibration band at $\sim 3000\text{-}2800\text{ cm}^{-1}$ reduced in intensity due to the loss of methyl-groups also belonging to TBMD-OTF group.

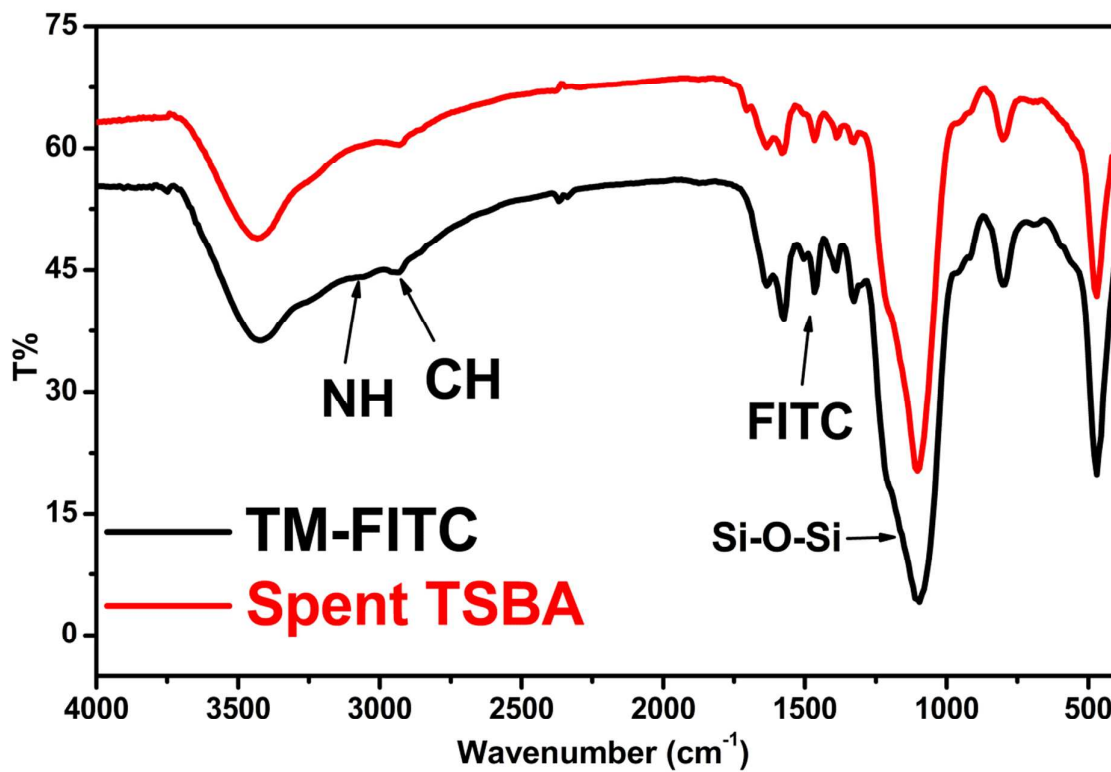


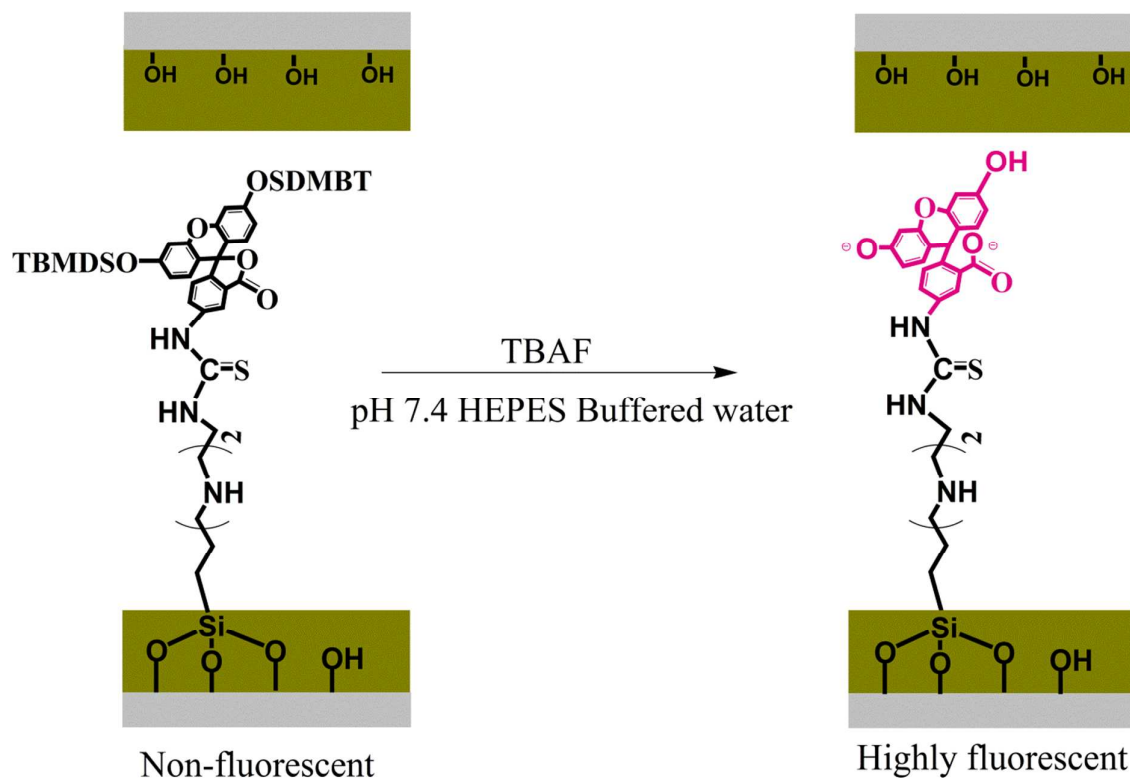
Fig. S4 IR spectra of spent TSBA and TM-FITC.

Moreover, we compared the spectra of the dried residue with that of TM-FITC (receptor **1** without TBMD-OTF). As expected, the two spectra look very similar (Fig. S4), suggesting that, the addition of F^- leads to the restoration of the fluorescein moiety.

Table 4EDX for as-prepared **TSBA** and spent **TSBA (s-TSBA)**.

Sample	Weight %				Atomic%			
	Carbon	Oxygen	Silicon	Sulfur	Carbon	Oxygen	Silicon	Sulfur
TSBA	49.50	40.62	8.90	0.98	61.01	34.43	3.96	0.60
s-TSBA	45.10	46.02	7.90	0.98	58.07	38.94	2.39	0.60

EDX analysis of the same solid residue corroborated the FT-IR results as shown in Table 4: the atomic % and weight % of silicon (Si) and carbon (C) content of the residue is lower compared to that of **TSBA**. Combine, we can confidently say that, a displacement reaction of fluoride at the Si-O center of TBMD-OTF took place to produce highly fluorescent fluorescein monoanions, which served as the fluorophore and chromophore responsible for the absorption and emission changes.³⁹ A schematic presentation of the above process is shown in scheme 2.



Scheme 2 Schematic illustration of the structure of **TSBA** and its selective detection of fluoride anion (the sensor: 88.0 mg mL^{-1} in pH 7.4 HEPES buffered water, fluoride anion: $1000 \text{ }\mu\text{M}$).

3.2.2. Selectivity performance of sensor

The selectivity of TSBA towards F^- over other anions was investigated by monitoring the fluorescence and absorption spectra of TSBA in the presence of other anions including HPO_4^{2-} , AcO^- , Cl^- , Br^- , I^- , and NO_3^- (in their tetrabutylammonium salt form). The comparison of the intensities is shown in Fig. S5 and Fig. 7. Clearly, only fluoride anions produced a mark improvement in fluorescence and absorption intensity at 526 nm and 496 nm respectively, whereas the addition of the anions under the same conditions produced almost

no change in intensity. The significant fluorescence amplification produced by F^- can be observed visually under both visible light and U-V light, as shown in Fig. 7(b).

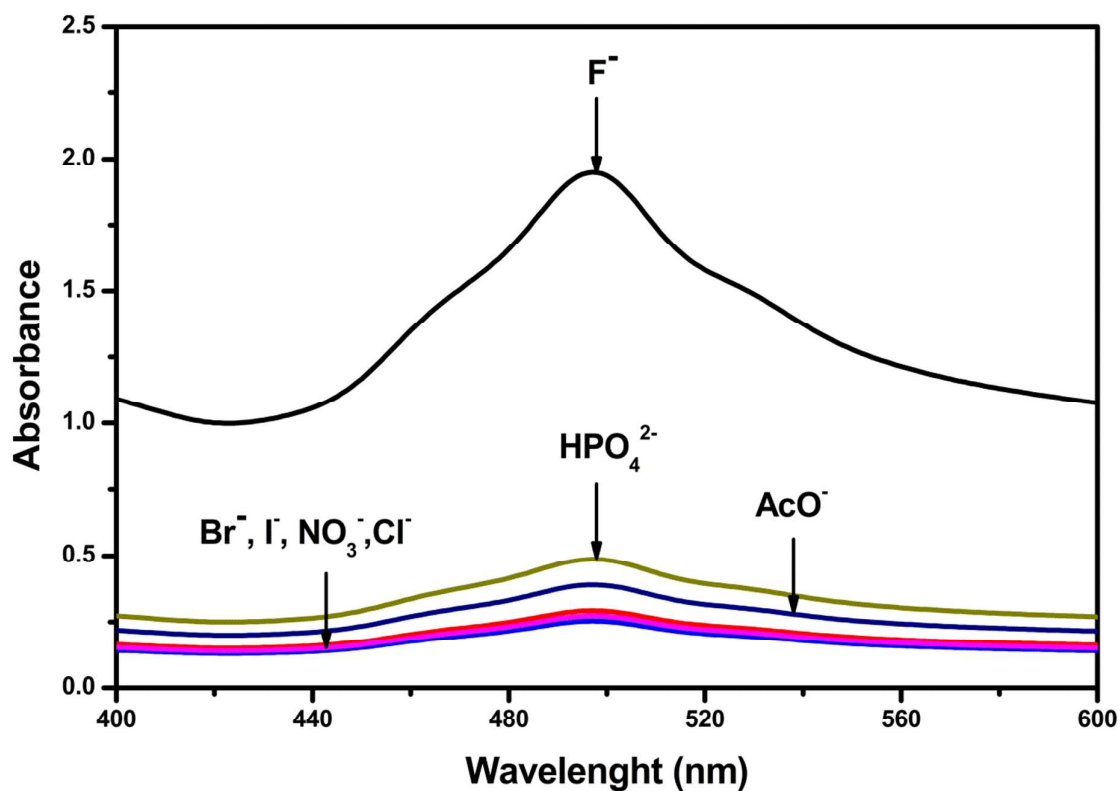
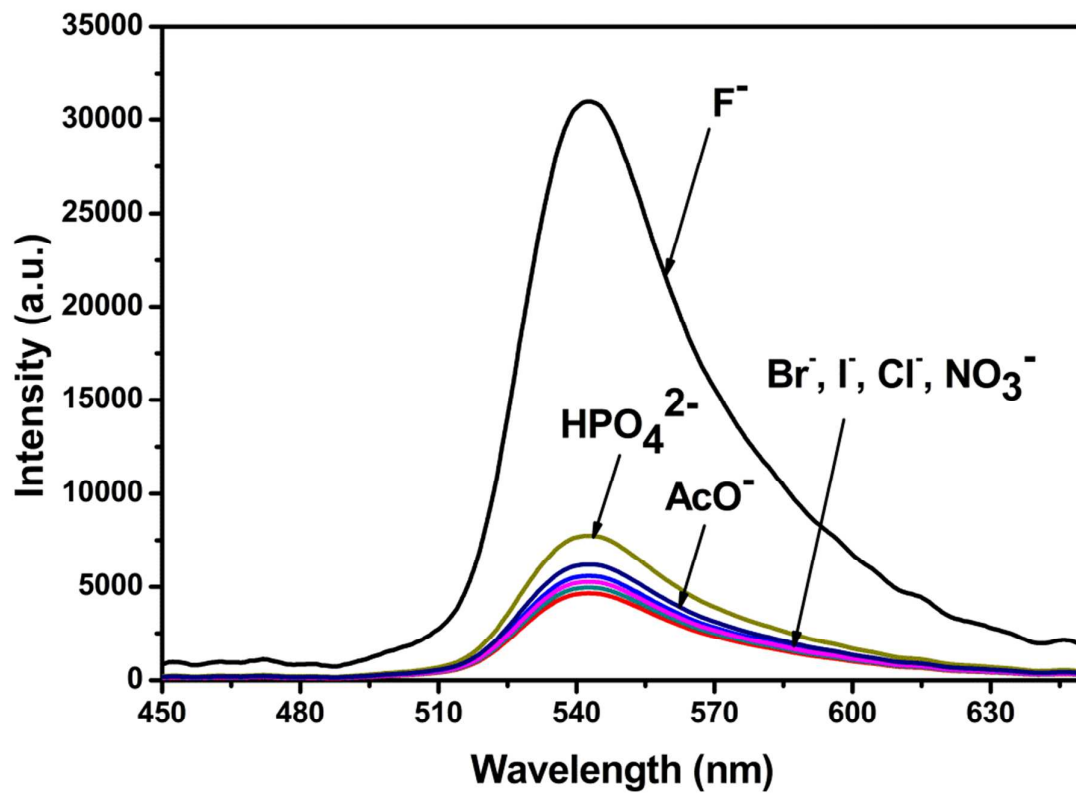
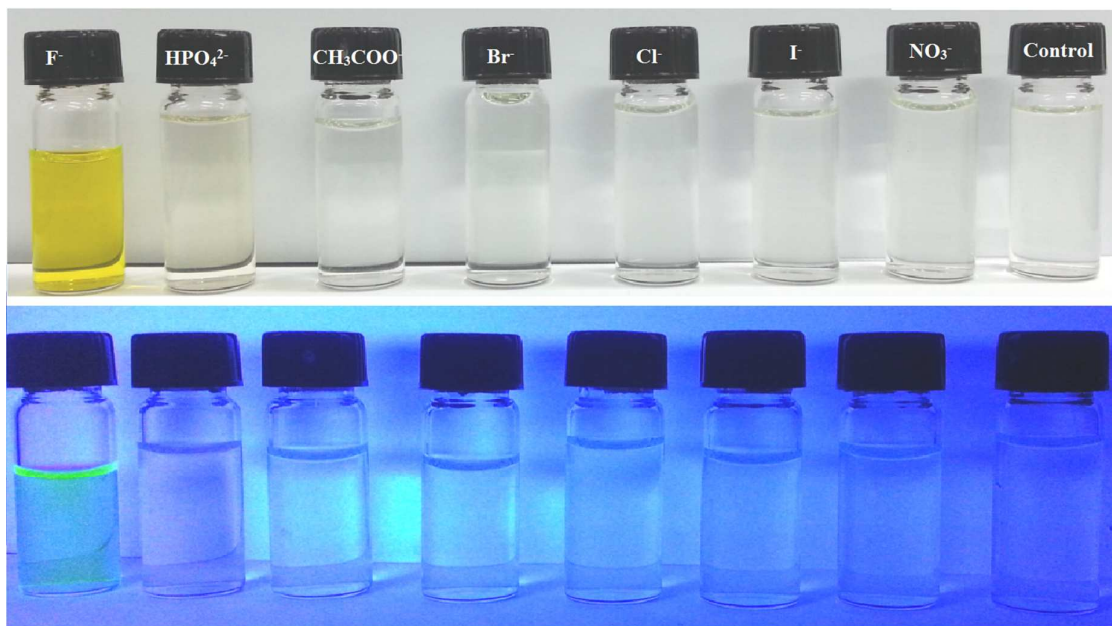


Fig. S5 Absorption spectra of TSBA (88.0 mg mL⁻¹) in 7.4 pH HEPES buffered water upon addition the same concentration of F^- , HPO_4^{2-} , AcO^- , Cl^- , Br^- , I^- , and NO_3^- .



(a)



(b)

Fig. 7 (a) Fluorescence spectra of **TSBA** (88.0 mg mL^{-1}) in 7.4 pH HEPES buffered water upon addition of the same concentration of F^- , HPO_4^{2-} , AcO^- , Cl^- , Br^- , I^- , and NO_3^- and (b) Photograph of solutions used in (a) under (top) visible light and (bottom) a hand-held UV light (352 nm).

The above results clearly showed that **TSBA** has an excellent selectivity towards fluoride anion over other common anions, especially HPO_4^{2-} and AcO^- , which have been reported to interfere with F^- detection.⁴⁰

A control experiment was conducted using **TM** and **TM-FITC**. Their fluorescence spectra in the absence and presence of F^- , HPO_4^{2-} , AcO^- , Cl^- , Br^- , I^- , and NO_3^- were recorded in water and 7.4 pH HEPES buffered water, respectively ; the comparison of the fluorescence intensities is shown in Fig. S6. As expected, **TM** showed no fluorescence spectra before and after the addition of anions. In addition, the pH of the water used remained relatively the same (~ 7), which suggested that the residual silanol groups on SBA-15 were not accessible to

the anions; and thus deprotonation reactions were avoided. The anions were therefore free from competing side reactions. **TM-FITC**, on the other hand, produced the same prominent emission spectra (ca. 30172.6156 a.u.) before and after the addition of anions; the intensity of which was similar to that of **TSBA** + 1000 μ M (ca. 29344.646), shown in Fig. 7(a). Based on the above results, it was concluded that the specific reaction between the F⁻ and the Si-O bond on receptor **1** was responsible for the prominent fluorescence observed in Fig. 7(b).

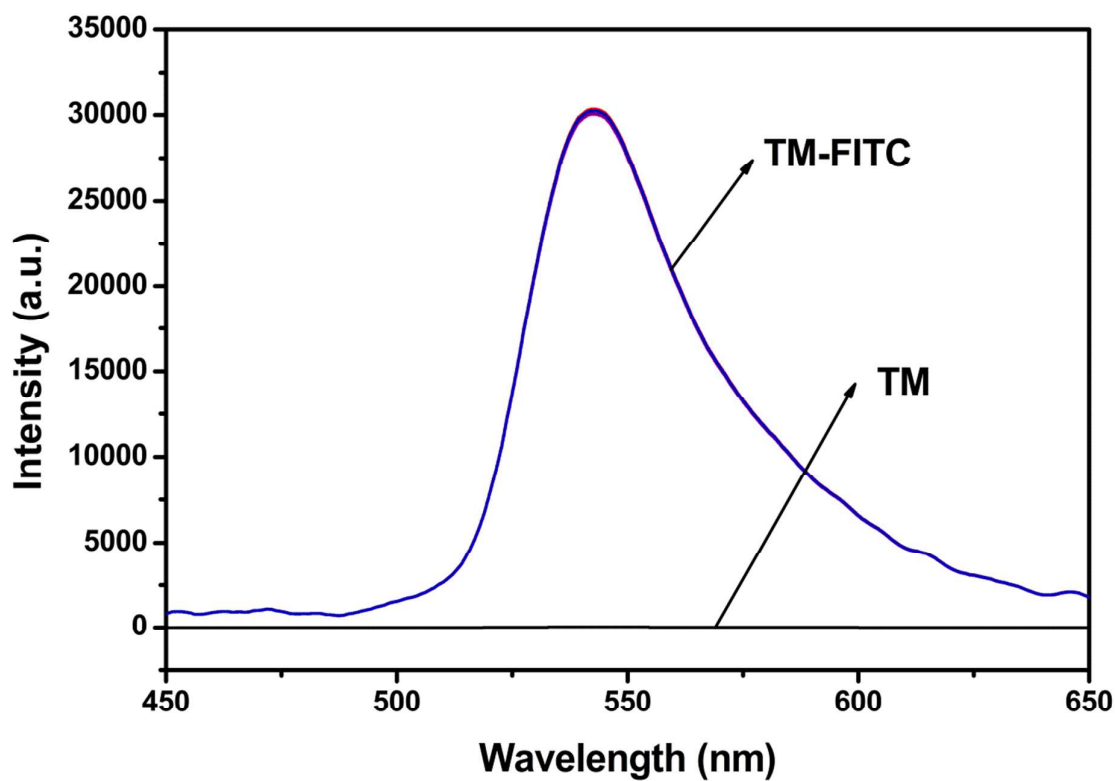
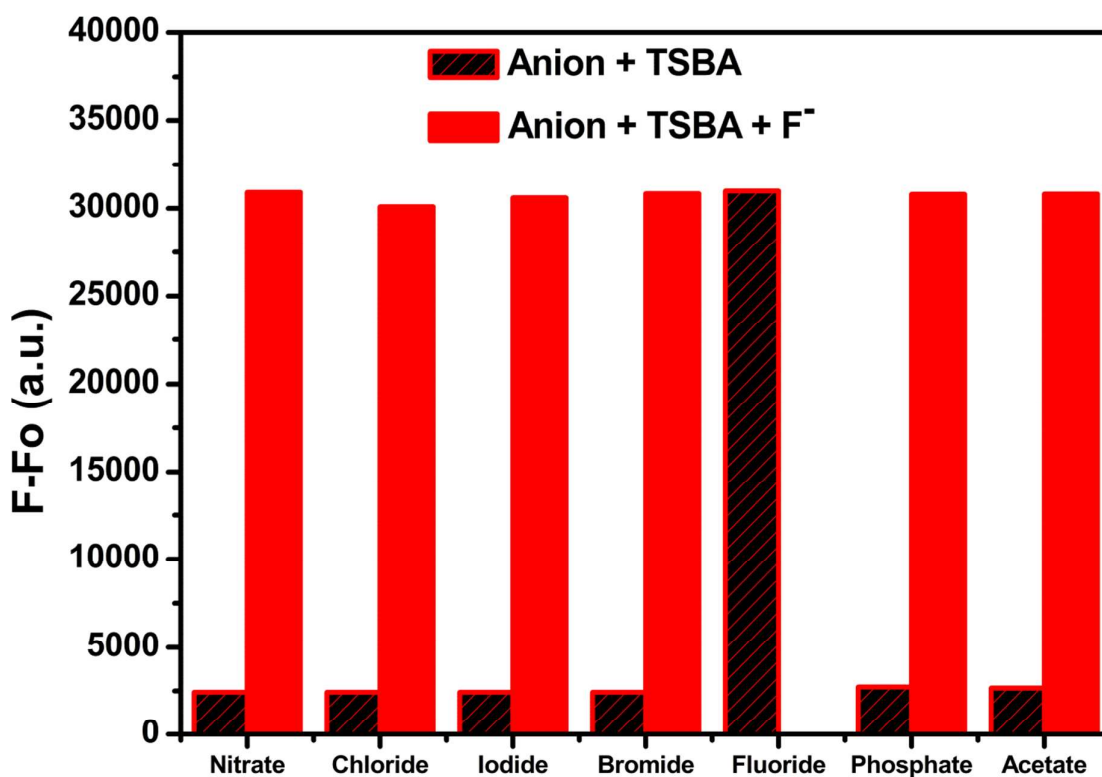


Fig. S6 Fluorescence spectra of **TM** and **TM-FITC** in the absence and presence of 1000 μ M solutions of F⁻, HPO₄²⁻, AcO⁻, Cl⁻, Br⁻, I⁻, and NO₃⁻.

The extent to which common anions interfere with the F^- sensing was also tested. Fig. 8 displays the fluorescence response of **TSBA** and **ASBA** to fluoride anions in the presence of other anions. It is clear that none of the **TSBA** and **ASBA** solutions containing HPO_4^{2-} , AcO^- , Cl^- , Br^- , I^- , and NO_3^- produced significant fluorescence until F^- was added. This meant that, the presence of these anions did not interfere with the reaction of F^- with **TSBA** and **ASBA**. We therefore concluded **TSBA** and **ASBA** can discriminate against F^- even in the presence of other anions; and hence, may function as a highly selective sensor for fluoride anions.



(b)

Fig. 8 Fluorescence intensities at 526 nm for **TSBA** (88.0 mg mL^{-1}) in the presence of $1000 \mu\text{M}$ of F^- and with the addition of $1000 \mu\text{M}$ of different anions respectively. ($\lambda_{\text{ex}} = 496 \text{ nm}$).

3.2.3. Photostability of sensor

To investigate whether **TSBA** remains stable under prolonged exposure to light, we recorded its fluorescence spectra with respect to time. Fig. 9 shows the fluorescence response of **TSBA** in the presence of 1.5 equiv. F^- continuously irradiated with a 30W UV- light source for 550 sec. The results show that, there was almost no photobleaching, as the fluorescence intensity value of **TSBA** changed by $\sim 0.12\%$. This sensor could therefore be applied in aqueous biological systems.

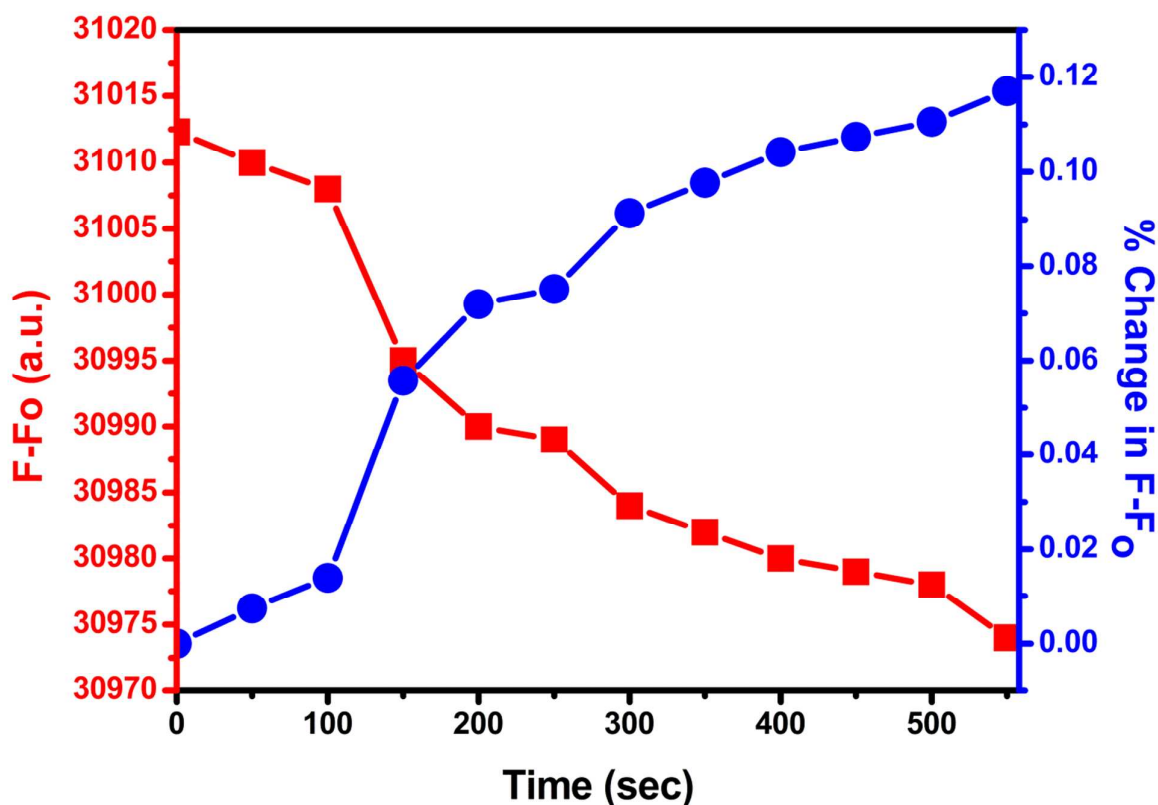


Fig. 9 A photobleaching experiment of **TSBA** (88.0 mg mL^{-1}) + 1.5 equiv. TBAF (in 7.4 pH HEPES buffered water) exposed to UV-light. The intensity values were measured at $\lambda_{\text{ex}} = 496 \text{ nm}$ and the % change in $F-F_0$ was cal. on the bases of $F-F_0$ at $T=0 \text{ sec}$.

4. Conclusion

In this work, we demonstrated that a silyl-ether protected fluorescein isothiocyanate (FITC) molecule (receptor **1**) could be successfully immobilized on amino-silane modified SBA-15 to give a robust fluorescent “turn-on” sensing system capable of detecting fluoride anions in totally aqueous media. We showed that, receptor **1** can be assembled in a “piece-wise” manner onto the surface of SBA-15 using a reaction method which excludes laborious purification steps. Furthermore, the as-prepared sensor demonstrated high sensitivity, photostability, selectivity, and response time values comparable to other reported F⁻ sensors. Finally, the incorporation of amino-alkoxysilane allowed us to control the sensitivity of the sensor, a feature which could open up the possibility of manipulating the detection limit of the sensor to meet specific demands.

Acknowledgement

This study was supported by National Research Foundation of Korea (NRF) – Grants funded by the Ministry of Science, ICT and Future Planning (2014R1A2A2A01004352) and the Ministry of Education (2009-0093816), Republic of Korea.

References

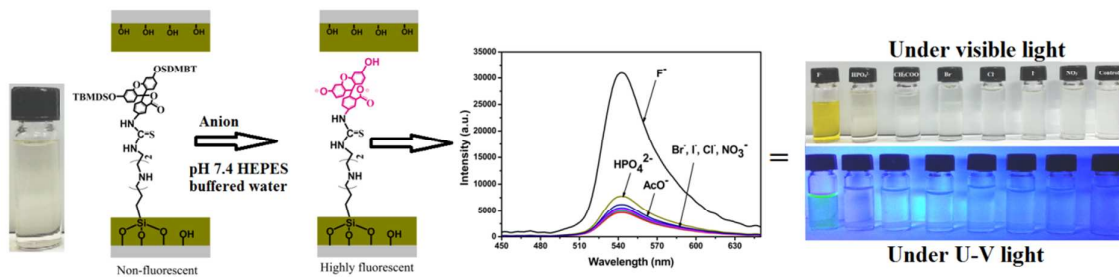
- 1 R. M. Duke, E. B. Veale, F. M. Pfeffer, P. E. Kruger and T. Gunnlaugsson, *Chem. Soc. Rev.*, 2010, **39**, 3936-3953.

- 2 (a) E. Galbraith and T. D. James, *Chem. Soc. Rev.*, 2010, **39**, 3831-3842; (b) V. Amendola, D. Esteban-Gomez, L. Fabbrizzi and M. Licchelli, *Acc. Chem. Res.*, 2006, **39**, 343-353; (c) P. A. Gale, *Coord. Chem. Rev.*, 2001, **213**, 79-128; (d) J. L. Sessler and J. M. Davis, *Acc. Chem. Res.*, 2001, **34**, 989-997.
- 3 (a) R. Martinez-Muñoz and F. Sancenón, *Chem. Rev.*, 2003, **103**, 4419-4776; (b) T. Gunnlaugsson, M. Glynn, G. M. Tocci, P. E. Kruger and F. M. Pfeffer, *Coord. Chem. Rev.*, 2006, **250**, 3094-3117; (c) Z. M. Hudson and S. Wang, *Acc. Chem. Res.*, 2009, **42**, 1584-1596.
- 4 (a) A. N. Swinburne, M. J. Paterson, A. Beeby and J. W. Steed, *Chem. Eur. J.*, 2010, **16**, 2714-2718; (b) Z. H. Zeng, A. A. J. Torriero, A. M. Bond and L. Spiccia, *Chem. Eur. J.*, 2010, **16**, 9154-9163.
- 5 M. Cametti and K. Rissanen, *Chem. Soc. Rev.*, 2013, **42**, 2016-2038.
- 6 Y. Zhou, J. F. Zhang and J. Yoon, *Chem. Rev.*, 2014, **114**, 5511-5571.
- 7 J. H. Clark, *Chem. Rev.*, 1980, **80**, 429-452.
- 8 (a) M. A. Reddy and M. Fichtner, *J. Mater. Chem.*, 2011, **21**, 17059-17062; (b) N. K. Subbaiyan, J. P. Hill, K. Ariga, S. Fukuzumi and F. D'Souza, *Chem. Commun.*, 2011, **47**, 6003-6005; (c) G. J.R. Cook, C. Parker, S. Chua, B. Johnson, A.-K. Aksnes and V. J. Lewington, *EJNMMI Res.*, 2011, **1**, 4-9; (d) Y. Li, C. Schiepers, R. Lake, S. Dadparvar and G. R. Berenji, *Bone*, 2012, **50**, 128-139; (e) W. Grochala, *J. Mater. Chem.*, 2009, **19**, 6949-6968; (f) A. Trewin, G. R. Darling and A. I. Cooper, *New J. Chem.*, 2008, **32**, 17-20.
- 9 (a) J. D. Dunitz and A. Gavezzotti, *Angew. Chem., Int. Ed.*, 2005, **44**, 1766-1787; (b) J. D. Dunitz and A. Gavezzotti, *Chem. Soc. Rev.*, 2009, **38**, 2622-2633; (c) A. Gavezzotti, *Acta Crystallogr., Sect. B: Struct. Sci.*, 2010, **66**, 396-406.

- 10 L. K. Kirk, *Biochemistry of the Halogens and Inorganic Halides*; Plenum Press: New York, 1991.
- 11 Kleerekoper and M. Endocrinol, *Metab. Clin. North Am.*, 1998, **27**, 441-452.
- 12 D. Briancon, *Rev. Rhum.*, 1997, **64**, 78-81.
- 13 (a) L. W. Ripa, *J. Publ. Health Dent.*, 1993, **53**, 17-44; (b) M. S. McDonagh, P. F. Whiting, P. M. Wilson, A. J. Sutton, I. Chestnutt, J. Cooper, K. Misso, M. Bradley, E. Treasure and J. Kleijnen, *Br. Med. J.*, 2000, **321**, 855-859; (c) C. Carstairs and R. Elder, *Can. Hist. Rev.*, 2008, **89**, 345-371.
- 14 Y. Michigami, Y. Kuroda, K. Ueda and Y. Yamamoto, *Anal. Chim. Acta.*, 1993, **274**, 299-302.
- 15 (a) E. Gazzano, L. Bergandi, C. Riganti, E. Aldieri, S. Doublier, C. Costamagna, A. Bosia and D. Ghigo, *Curr. Med. Chem.*, 2010, **17**, 2431-2441; (b) B. Spittle, *Fluoride*, 2011, **44**, 117-124; (c) P. Grandjean and P. J. Landrigan, *Lancet*, 2006, **368**, 2167-2178; (d) O. Barbier, L. Arreola-Mendoza and L. M. Del Razo, *Chem.-Biol. Interact.*, 2010, **188**, 319-333; (e) R. Sandhu, H. Lal, Z. S. Kundu and S. Kharb, *Bio. Trace Elem. Res.*, 2011, **144**, 1-5; (f) M. C. Friesen, G. Benke, A. Del Monaco, M. Dennekamp, L. Fritschi, N. de Klerk, J. L. Hoving, E. MacFarlane and M. R. Sim, *Cancer, Causes Control, Pap. Symp.*, 2009, **20**, 905-916.
- 16 S. Jagtap, M. K. Yenkie, N. Labhsetwar and S. Rayalu, *Chem. Rev.*, 2012, **112**, 2454-2466.
- 17 A. Bhatnagar, E. Kumar and M. Sillanpää, *Chem. Eng. J.*, 2011, **171**, 811-840; P. Miretzky and A. F. Cirelli, *J. Fluorine Chem.*, 2011, **132**, 231-240.
- 18 P. Cosentino, B. Grossman, C. Shieh, S. Doi, H. Xi and P. Erbland, *J. Geotech. Eng.*, 1995, **121**, 610-617.

- 19 T. W. Hudnall, C.-W. Chiu and F. P. Gabbaï, *Acc. Chem. Res.*, 2009, **42**, 388-397.
- 20 P. Konieczka, B. Zygmont and Namiesnik, *J. Bull. Environ. Contam. Toxicol.*, 2000, **64**, 794-803.
- 21 K. Itai and H. Tsunoda, *Clin. Chim. Acta.*, 2001, **308**, 163-171.
- 22 E. Palomares, R. Vilar, A. Green and J. R. Durrant, *Adv. Funct. Mater.*, 2004, **14**, 111-115.
- 23 A. P. Wight and M. E. Davis, *Chem. Rev.*, 2002, **102**, 3589-3614.
- 24 E. Topoglidis, C. J. Campbell, E. Palomares and J. R. Durrant, *Chem. Commun.*, 2002, **14**, 1518-1519.
- 25 C.-Y. Lai, B. G. Trewyn, D. M. Jefthinija, K. Jefthinija, S. Xu, S. Jefthinija and V. S.-Y. Lin, *J. Am. Chem. Soc.*, 2003, **125**, 4451-4459.
- 26 M. Numata, C. Li, A.-H. Bae, K. Kaneko, K. Sakurai and S. Shinkai, *Chem. Commun.*, 2005, **37**, 4655-4657.
- 27 S. J. Lee, S. S. Lee, M. S. Lah, J.-M. Hong and J. H. Jung, *Chem. Commun.*, 2006, **42**, 4539-4541.
- 28 S. J. Lee, S. S. Lee, J. Y. Lee and J. H. Jung, *Chem. Mater.*, 2006, **18**, 4713-4715.
- 29 S. J. Son and S. B. Lee, *J. Am. Chem. Soc.*, 2006, **128**, 15974-15975.
- 30 T. Balaji, S. A. El-Safty, H. Matsunaga, T. Hanaoka and F. Mizukami, *Angew. Chem., Int. Ed.*, 2006, **45**, 7202-7208.
- 31 E. Kim, H. J. Kim, D. R. Bae, S. J. Lee, E. J. Cho, M. R. Seo, J. S. Kim and J. H. Jung, *New J. Chem.*, 2008, **32**, 1003-1007.
- 32 X. Feng, G. E. Fryxell, L.-Q. Wang, A. Y. Kim, J. Liu and K. M. Kemner, *Science*, 1997, **276**, 923-926.
- 33 X. Wang, P. Wang, Z. Dong, Z. Ma, J. Jiang, R. Li and J. Ma, *Nanoscale Res Lett.*,

- 2010, **5**,1468-1473.
- 34 P. Vejayakumaran, I. A. Rahmana, C. S. Sipaut, J. Ismail and C.K. Chee, *J. Colloid Interface Sci.*, 2008, **328**, 81-91.
- 35 S. EK, A.Root, M. Peussa and L. Niinisto, *Thermochem. Acta.*, 2001,**379**, 201-212.
- 36 H. Ritter, J. H. Raman and D. Bruhwiler, *Materials*, 2010, **3**, 4500-4509.
- 37 S. J. Lee, S. S. Lee, J. Y. Lee and J. H. Jung, *Chem. Mater.*, 2006, **18**, 4713-4715.
- 38 F. Gao, F. Luo, J. Yin and L. Wang, *Luminescence*, 2008, **23**, 392-396.
- 39 F. Zheng, F. Zeng, C. Yu, X. Hou and S. Wu, *Chem. Eur. J.*, 2013, **19**, 936- 942.
- 40 P. Sokkalingam and C.-H. Lee, *J. Org. Chem.*, 2011, **76**, 3820-3828.
- 41 V. Thomsen, D. Schatzlein and D. Mercurio, *Spectroscopy*,2003, **18**, 112-114.
- 42 J. Ren, Z. Wu, Y. Zhou, Y. Li and Z. Xu, *Dyes and Pigments*, 2001, **91**, 442-445.
- 43 Y. Chen, W. Shi, Y. Hui, X. Sun, L. Xu, L. Feng and Z. Xie, *Talanta*, 2015, **137**, 38-42.
- 44 X.-F. Yang, H. Qi, L. Wang, Z. Su and G. Wang, *Talanta*, 2009, **80**, 92-97.



TSBA (or ASBA) remained stable under prolonged exposure to UV light (losing $\sim 0.12\%$ of its fluorescence intensity), and was highly selective towards F^- over other common anions (Cl^- , Br^- , I^- , HPO_4^{2-} , AcO^- , and NO_3^-).